buildings

MDPI

Article

Data Center Energy Evaluation Tool Development and Analysis of Power Usage Effectiveness with Different Economizer Types in Various Climate Zones

Ji Hye Kim [1], Dae Uk Shin [2] and Heegang Kim [3,*]

[1] Department of Architectural Engineering, Kwangwoon University, 20 Kwangwoon-ro, Seoul 01897, Republic of Korea; jikim@kw.ac.kr
[2] Department of Architecture and Building Engineering, Kunsan National University, 558 Daehak-ro, Gunsan, Jeonbuk 54150, Republic of Korea; daeuk.shin@kunsan.ac.kr
[3] Plant Research Group, Posco E&C, 241 Incheon Tower-daero, Incheon 22009, Republic of Korea
* Correspondence: hgkim_etoile@poscoenc.com; Tel.: +82-32-748-1833

Abstract: Data centers are energy-intensive facilities, with over 95% of their total cooling load attributed to the heat generated by information technology equipment (ITE). Various energy-saving techniques have been employed to enhance data center efficiency and to reduce power usage effectiveness (PUE). Among these, economizers using outdoor air for cooling are the most effective for addressing year-round cooling demands. Despite the simplicity of the load composition, analyzing data center cooling systems involves dynamic considerations, such as weather conditions, system conditions, and economizer control. A PUE interpretation tool was specifically developed for use in data centers, aimed at addressing the simplicity of data center loads and the complexity of system analysis. The tool was verified through a comparison with results from DesignBuilder implementing the EnergyPlus algorithm. Using the developed tool, a comparative analysis of economizer strategies based on the PUE distribution was conducted, with the aim of reducing the PUE of data centers across various climatic zones. The inclusion of evaporative cooling (EC) further improved cooling efficiency, leading to reductions in PUE by approximately 0.02 to 0.05 in dry zones. Additionally, wet zones exhibited PUE reductions, ranging from approximately 0.03 to 0.07, with the implementation of indirect air-side economizer (IASE). Sensitivity and uncertainty analysis were further conducted. The computer room air handler (CRAH) supply temperature and CRAH temperature difference were the most influential factors affecting the annual PUE. For the direct air-side economizer (DASE) and DASE + EC systems, higher PUE uncertainty was observed in zones 1B, 3B, 4B, and 5B, showing ranges of 1.17–1.39 and 1.15–1.17, respectively. In the case of the IASE and IASE + EC systems, higher PUE uncertainty was noted in zones 0A, 0B, 1A, 1B, and 2A, with ranges of 1.22–1.43 and 1.17–1.43, respectively. The distinctive innovation of the tool developed in this study is characterized by its integration of specific features unique to data centers. It streamlines the computation of cooling loads, thus minimizing the burden of input, and delivers energy consumption data for data center cooling systems with a level of precision comparable to that of commercial dynamic energy analysis tools. It provides data center engineers with a valuable resource to identify optimal alternatives and system design conditions for data centers. This empowers them to make informed decisions based on energy efficiency enhancements, thereby strengthening their ability to improve energy efficiency.

Keywords: data centers; power usage effectiveness (PUE); energy evaluation tool; economizer; sensitivity and uncertainty analysis

Citation: Kim, J.H.; Shin, D.U.; Kim, H. Data Center Energy Evaluation Tool Development and Analysis of Power Usage Effectiveness with Different Economizer Types in Various Climate Zones. *Buildings* **2024**, *14*, 299. https://doi.org/10.3390/buildings14010299

Academic Editors: Yu Huang, Siwei Lou and Yukai Zou

Received: 24 November 2023
Revised: 19 January 2024
Accepted: 20 January 2024
Published: 22 January 2024

1. Introduction

The expansion of cloud computing technology, which provides computing resources over the internet, along with the explosive development of data-intensive technologies, such as big data and artificial intelligence, has increased the demand for high-density data

centers. According to the International Energy Agency (IEA), the estimated global electricity consumption by data centers in 2022 was between 240 and 340 TWh [1], accounting for approximately 1–1.5% of the total global electricity consumption across all sectors. [2–4]. Given this considerable energy consumption, data centers are actively pursuing strategies to improve their energy efficiency [5,6].

Power usage effectiveness (PUE) is a key metric used in the data center industry for assessing energy efficiency [7], which measures the ratio of the total energy consumed by the facility to the amount of energy consumed by the information technology equipment (ITE), where lower PUE values indicate a superior energy usage efficiency. Cooling systems play a particularly substantial role in the energy consumption of data centers, accounting for approximately 30–50% of the total electrical energy used in data centers [8–11]. Efforts to decrease the PUE often focus on reducing cooling energy consumption through various energy-saving cooling configurations.

Data centers experience year-round cooling loads, with IT heat generation contributing to over 95% of the total cooling load [12]. This characteristic significantly influences the energy-saving strategies of data center cooling systems. To satisfy consistent cooling requirements, data centers implement economizers that leverage outdoor air for cooling process [13–27]. This approach curtails the operational hours of chillers, which are the most energy-intensive components of cooling systems, which results in substantial energy savings. In addition, given the presence of only a sensible heat load, no requirement is present for the dehumidification of the cooling coil, which can increase the chilled water supply temperature to a computer room air handler (CRAH). This phenomenon not only enhances the chiller efficiency but also extends the operational timeframe of the water-side economizer (WSE), leading to reduced power consumption in the water loop. Furthermore, relaxing the recommended temperature and humidity standards for server rooms presents a chance to increase both the CRAH supply temperature and the chilled water supply temperature [28]. Consequently, the operational duration of the economizer is extended, creating additional potential for substantial reductions in cooling energy consumption. Collectively, these measures contribute to the overall enhancement of the energy efficiency of data center cooling systems.

Conducting a dynamic cooling energy analysis is vital to effectively assess the energy efficiency of data centers using economizers. Such an analysis involves considering the operation of the economizer in response to changing outdoor weather conditions and variations in equipment performance under diverse operational circumstances, including the cooling medium temperature and part load ratio (PLR). While commercial building energy analysis programs (e.g., TRNSYS and EnergyPlus) are commonly used in data center cooling energy analysis [13,17,21,24,29,30], these existing tools were initially designed to handle a wide range of building and system scenarios, which has resulted in complex and intricate system modeling and inputs. Consequently, engineers may encounter challenges when using commercial programs to explore alternative options during the initial design stages. Despite the necessity for detailed system modeling in energy analysis, a significant advantage in the study of data center cooling is that the cooling loads are largely driven by the heat produced by ITE; thus, the load calculations are simplified. In this regard, a specialized tool has been developed for use in energy analysis and PUE calculations in data centers. This tool, being specifically designed for data center applications, yields considerable benefits. These dedicated tools enable engineers to conduct precise energy analyses with enhanced ease and efficiency, by considering the unique characteristics of data center cooling systems.

Several studies have focused on analyzing the PUE in data centers, with a specific emphasis on utilizing economizers to achieve energy efficiency and savings [18,19,29–37]. For example, Gozcü et al. [29] conducted a data center PUE analysis of four economizer types in 19 selected cities based on the American Society of Heating, Refrigerating and Air-Conditioning Engineers (ASHRAE) climate zone [38]. Although their research offered a comprehensive assessment of the PUE and accounted for various economizer types and

their performance across different climate zones, the study was limited in terms of the system design conditions. Specifically, the study concentrated solely on two scenarios of CRAH supply air temperatures (15 °C and 25 °C), providing a limited scope for analyzing diverse cooling strategies. Consequently, the findings of this study may not have fully captured the potential impact of economizers under a wider range of operating conditions and cooling system designs. Therefore, to gain a more comprehensive understanding of economizer effectiveness, further studies are required to explore a broader range of design parameters and operating conditions.

Cho et al. [34] developed a DCeET simulation tool designed specifically for data centers, which enables the evaluation of three economizer alternatives: direct air-side economizer (DASE), indirect air-side economizer (IASE), and WSEs. By leveraging hourly weather data, the tool captures the dynamic nature of the energy performance of the data center, which is crucial for conducting an accurate analysis. In another study [18], researchers investigated the combined use of DASE and WSE in ten Iranian cities to enhance the PUE. A thermodynamic-based model was utilized to evaluate the impact of these economizer types on the energy efficiency of data centers. However, neither this study nor the DCeET tool designed by Cho et al. [34] considered the impact of the PLR and cooling medium (air or water) temperatures on equipment performance and conducting an energy analysis in data centers. Incorporating these factors could offer a comprehensive and accurate understanding of data center energy efficiency and further optimize the cooling system design. Mi et al. [39] conducted a study investigating the discrepancies between field test results of data centers employing water side economizers and their analysis under ideal conditions. A key factor identified for these differences was the fluctuation in cooling water temperatures, which are affected by changes in outdoor wet-bulb temperature during the use of economizers. To address this effect, the study utilized a chiller energy model that took into account the PLR and the fluctuations in cooling water temperature. The study of Lei et al. [35] conducted a predictive analysis of data center PUE, focusing on hyperscale data centers and considering three economizer methods: DASE, WSE, and seawater-based economizers. The study involved predicting the PUE values for 17 hyperscale data centers operated by Google and Facebook. This study accounted for location-specific weather conditions, uncertainties in energy system parameters, and economizer choices. However, although their PUE calculations focused on the impact of the PLR and the temperatures of the chilled water and cooling water on the chiller performance, this study overlooked the influence of the PLR on the power calculations of the CRAH fan. Notably, economizers can reduce the chiller operation time, leading to a higher proportion of energy consumption by the continuously operating CRAH fan, which is based on the IT load. Accurate calculations of the power usage of the CRAH fan in economizer-based systems are crucial when conducting a comprehensive energy analysis of data center cooling systems.

The primary objective of this study was to develop 'DCSim', a dynamic energy analysis tool tailored specifically for data centers. The innovation of DCSim lies in its ability to integrate the unique characteristics of data centers. This tool simplifies the process of calculating cooling loads, reducing the burden on users, and provides energy consumption results for data center cooling system configurations with an accuracy comparable to commercial dynamic energy programs. In its energy analysis, DCSim considers variations in cooling medium temperatures and the part load ratio (PLR) of essential components such as fans, pumps, and chillers. These aspects have been only partially addressed in previous data center research. A key feature of DCSim is its capability to accurately assess PUE, taking into account the impact of various cooling system configurations and equipment parameters under various weather conditions. DCSim provides engineers with a sophisticated tool necessary for determining the most efficient system designs and alternatives for data centers during the design phase, significantly contributing to decision-making processes that enhance energy efficiency.

2. Materials and Methods

This study is structured in four steps. In the initial two steps, commonly employed systems within data centers are introduced, and a system model is proposed for dynamically calculating PUE. This model takes into account the dynamic fluctuations in cooling requirements, outdoor weather conditions, and various system parameters. The third step involves the validation of the developed program, utilizing results obtained from DesignBuilder (Version 7.0.2.4), a commercial dynamic energy analysis program. Finally, in the fourth step, an in-depth analysis of PUE based on economizer configurations in different climate regions is conducted. This step includes a sensitivity analysis to assess the impact of various system design parameters on PUE. Subsequently, the research focuses on evaluating the uncertainties in PUE related to economizer types and climate regions, with particular emphasis on the influential system parameters in this context (Figure 1).

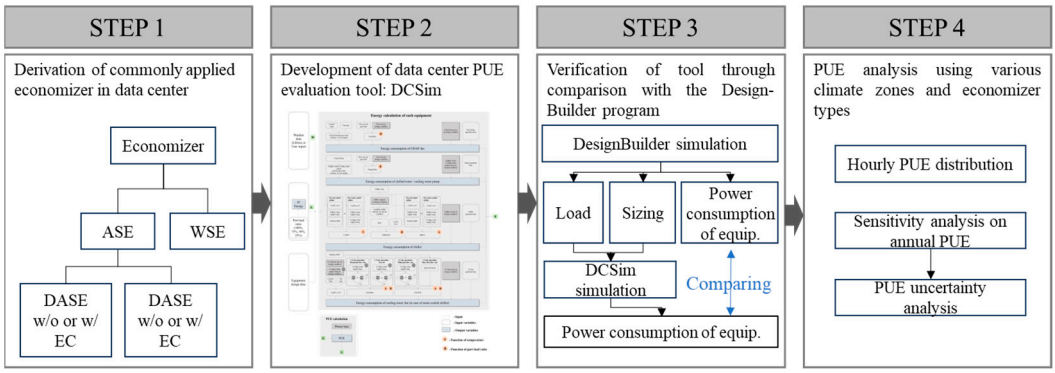

Figure 1. Research procedure.

2.1. DCSim

DCSim, specifically developed for engineers, emerges as an innovative tool aimed at enhancing the analysis of cooling energy and PUE in data center projects. This program distinctively addresses the specialized load characteristics and operational dynamics of cooling systems within data center, distinguishing them from conventional buildings. It is ingeniously structured to compute PUE, taking into account the diverse quantities and degrees of information available at various stages of a project.

Data centers, with their inherent need for continuous cooling, encounter dynamic shifts in cooling water temperatures during winter, influenced by the external ambient temperature. When utilizing WSE, operational adjustments, such as elevating the chilled water temperature, are often implemented to extend the economizer's effective period. This operation, diverging from traditional building cooling systems, requires running under different thermal conditions. Consequently, there arises a need for an analytical assessment of cooling energy consumption that takes into consideration the varying efficiency of the system in response to these shifts in ambient temperatures. This analytical approach is essential for accurately evaluating and optimizing the energy performance of data center cooling systems, which operate under a set of conditions markedly different from conventional building environments.

In the construction industry, the procurement phase of data center projects mandates that companies stringently evaluate the possibility of achieving the PUE targets set by clients. Subsequently, the design phase requires a comprehensive assessment of PUE, integrating the performance attributes of the equipment selected by the design company. This evaluation is crucial for effective project quality management. To adeptly cater to this requirement, the program has been meticulously designed to perform PUE calculations grounded in the detailed evolution of information available at each stage of the project. Initially, during the bidding phase, the available data often pertains only to the total capacity of IT equipment or the generic type of the cooling system. Anticipating this limitation, a comprehensive library of performance data has been established to facilitate the evaluation

of equipment performance, influenced by factors such as load ratios and temperature variables, even before specific equipment specifications are determined.

As the project progresses and both the cooling system configuration and equipment specifications become finalized, the program is structured to allow users to input specific performance data of the selected equipment. This feature enables the execution of precise and customized PUE calculations, aligning with the actual system configuration and ensuring an accurate reflection of the project's energy efficiency potential.

The DCSim program has been developed using MATLAB, and its input and output interfaces depicted in Figure A1 (in Appendix B) The input interface of the program divided into two sections: one for the input of weather data and load-related information, and the other for entering parameters related to the cooling system. The weather data can be either selected from a predefined library or entered manually by the user. In consideration of the typical characteristics of data centers, where IT heat load often accounts for over 90% of the total load, the input for load calculations has been streamlined. Users are required to input rack-level heat density, the number of racks, as well as external loads and lighting heat density on a per-unit area basis, with the aim of simplifying the load input process.

In the section dedicated to input parameters for the cooling system, users are provided with the capability to specify system configurations and equipment parameters. Within the system configuration input section, users can select one or multiple of the eight cooling systems commonly employed in large-scale data centers, denoted as Case 1 through Case 8 in Figure A1. This selection allows for the ease of comparative analysis when multiple systems are chosen. In the equipment parameter input section, users are afforded the flexibility to either select parameters from a predefined library or input them manually.

Considering that data centers may operate for extended periods at less than 50% load in the initial stages, before server installation is completed, it becomes essential to assess cooling energy consumption and PUE levels under partial load conditions. Therefore, the program offers the flexibility to perform analysis and comparative reviews for four default load levels (100%, 75%, 50%, 25%), as well as specific load levels as required by the user. Users are provided with the option to select the desired load level for comparative analysis and review within the input interface.

The program's output interface consists of three distinct display windows. In the first window, graphs of the weather data used in the calculations are presented. Subsequently, the second and third windows provide concise graphical and tabular summaries, encompassing monthly cooling energy consumption, the operational durations of free cooling, mixed cooling, and mechanical cooling modes when the economizer is in operation, along with the results for PUE. These summarizing visuals are tailored for rapid reference and are additionally accessible in an hourly-based format, thus promoting comprehensive and in-depth analysis.

2.2. System Description

Traditional cooling systems in data centers, consisting of CRAH units and mechanical vapor compression chillers, consumes a significant amount of cooling energy to dissipate the heat generated by the ITE. The continuous year-round operation of chillers, regardless of outdoor temperature conditions, can lead to substantial energy consumption and inefficiencies in data center cooling. To address this issue and reduce cooling energy usage, data centers have implemented various techniques, including containment solutions, optimized perforated tiles, expanded server room temperature and humidity ranges, and economizers. Among these techniques, economizers have proven to be highly effective in significantly reducing cooling energy usage.

Most data centers design and operate their cooling systems based on the ASHRAE's "Thermal Guidelines for Data Processing Environments" [28], which were first published in 2004 and subsequently updated in 2008, 2011, and 2015. Each update extended the environmental envelope ranges in response to the increased environmental tolerance of newer generations of IT hardware and the growing emphasis on cooling energy savings. These

expanded ranges have provided data center operators with opportunities to save energy by increasing operating temperatures, adjusting humidity ranges, and allowing longer periods of economizer usage. Consequently, relaxed indoor temperature and humidity conditions with economizer applications have significantly improved the effectiveness of economizers, whose implementation is a crucial aspect of recent data center cooling systems.

The three most common economizers used in data centers are as follows:

- Direct Air-Side Economizer (DASE) [13–19,23,25,26]: Figure 2a shows a schematic of the DASE. This approach involves introducing a specific quantity of outside air (OA) directly into a server room when the temperature and humidity of the outdoor air meet cooling requirements. The operation of the DASE is influenced by the outdoor temperature as well as its humidity and quality.
- Indirect Air-Side Economizer (IASE) [13,17,23,25,26]: An IASE employs an air-to-air heat exchanger, as depicted in Figure 2b, to facilitate heat exchange between the indoor and outdoor air while preventing direct mixing. Although the efficiency of the heat exchanger limits the full utilization of the outdoor air heat, the IASE extends the period of free cooling compared with that in the DASE because it is unaffected by the outdoor air humidity or air quality.
- Water-Side Economizer (WSE) [16,18–24,26]: The WSE cools the data center using a water-to-water heat exchanger, as shown in Figure 2c. When the outdoor air temperature is sufficient, the chiller can either be bypassed or the heat exchanger can first lower the chilled-water temperature and the chiller can then compensate for the remaining cooling needs.

Both the DASE and IASE implement evaporative cooling (EC) on the OA side to lower the OA temperature and extend the duration of the free-cooling operation, as shown in Figure 2a,b.

2.3. Economizer Operation Modes

Economizer operation modes are categorized into three types based on outdoor conditions: free cooling, mixed cooling, and mechanical cooling. In the free cooling mode, the chiller is inactive when the outdoor conditions are suitable for cooling using OA alone. In the mixed cooling mode, the data center is partially cooled using OA and the chiller when the desired indoor temperature cannot be maintained solely by OA. When the outdoor conditions are unsuitable for economizer operation, the mechanical cooling mode is operated, and cooling is performed exclusively by the chiller.

For DASE operation, the decision is determined by the outdoor dry-bulb temperature ($T_{OA,DB}$), outdoor dew point temperature ($T_{OA,DPT}$), low-limit temperature ($T_{DB,lowlimit}$, generally the CRAH supply temperature), and high-limit temperature ($T_{DB,highlimit}$, generally the CRAH return temperature), as shown in Figure 3a. In the free cooling mode, if $T_{OA,DPT}$ is below the upper limit (15 °C) of ASHRAE's recommended range and $T_{OA,DB}$ is lower than $T_{DB,lowlimit}$, the DASE system combines return air (RA) and OA to handle the cooling load without involving the chiller. In the mixed cooling mode, when $T_{OA,DPT}$ is below the upper limit and $T_{OA,DB}$ falls within the range of $T_{DB,lowlimit}$ and $T_{DB,highlimit}$, DASE introduces 100% OA into the space and the chiller operates to maintain the supply air (SA) set points. In the mechanical cooling mode, if $T_{OA,DPT}$ are above the upper limit or $T_{OA,DB}$ exceeds $T_{DB,highlimit}$, the system recirculates air without mixing in the OA, and the chiller cools the RA to remove the cooling load.

The determining factors for IASE operation are $T_{OA,DB}$, $T_{DB,lowlimit}$, and $T_{DB,highlimit}$, as illustrated in Figure 3b. In the free cooling mode, when $T_{OA,DB}$ is lower than $T_{DB,lowlimit}$, RA is indirectly cooled using the OA induced by the exhaust (EA) fan, thereby maintaining the SA temperature set point without chiller operation. In the mixed cooling mode, if $T_{OA,DB}$ is higher than $T_{DB,lowlimit}$ but lower than $T_{DB,highlimit}$, the exhaust fan operates at the maximum airflow to reduce the cooling load, and the chiller maintains the SA temperature. In the mechanical cooling mode, when $T_{OA,DB}$ exceeds $T_{DB,highlimit}$, the RA bypasses the heat exchanger, and the chilled water system handles all cooling loads.

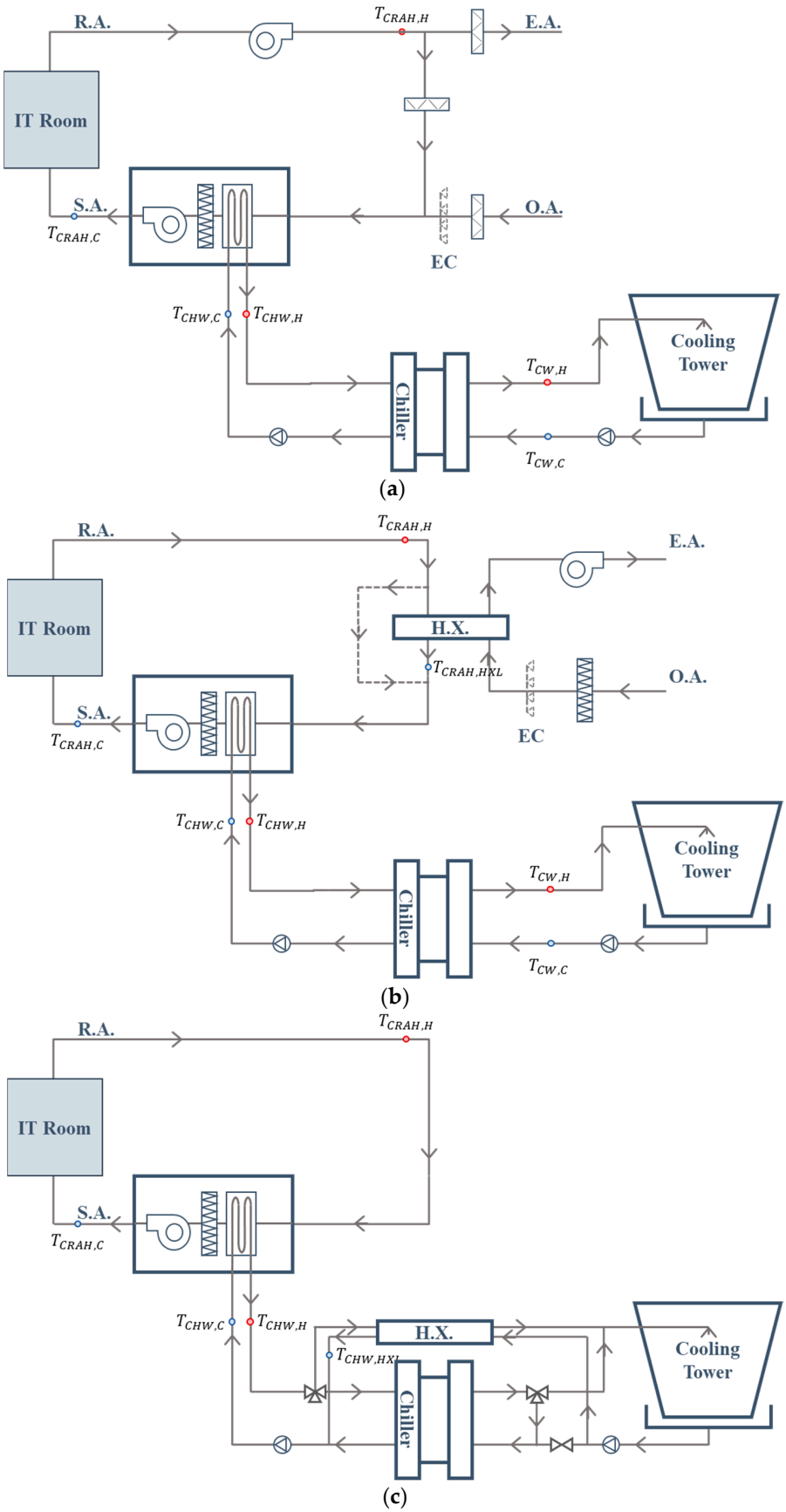

Figure 2. Schematics of economizer-utilizing cooling systems: (**a**) Direct air-side economizer (DASE); (**b**) indirect air-side economizer (IASE); (**c**) water-side economizer (WSE).

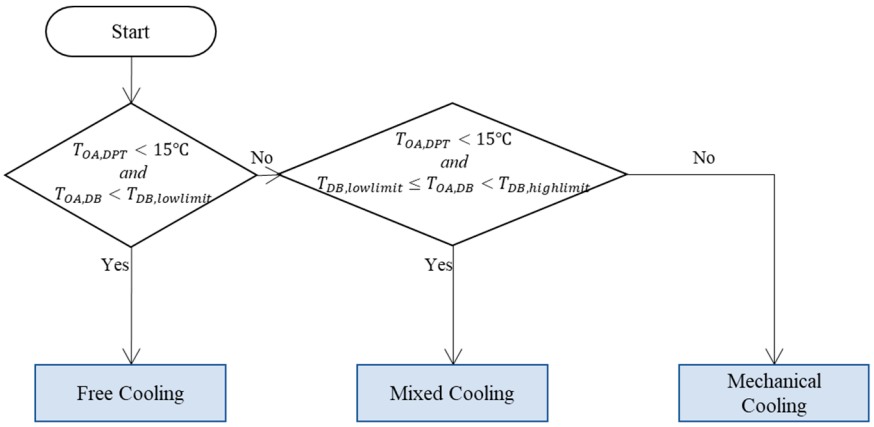

* For evaporative cooling $T_{OA,EDB}$ instead of $T_{OA,DB}$ where, $\epsilon_{EC} = \frac{T_{OA,DB} - T_{OA,EDB}}{T_{OA,DB} - T_{OA,WB}}$

$T_{OA,DPT}$: Outdoor dew point temp.[℃]
$T_{OA,DB}$: Outdoor dry-bulb temp. [℃]
$T_{OA,WB}$: Outdoor wet bulb temp.[℃]
$T_{DB,lowlimit}$: Economizer low limit dry-bulb temp. [℃]
$T_{DB,highlimit}$: Economizer high limit dry-bulb temp. [℃]

(**a**)

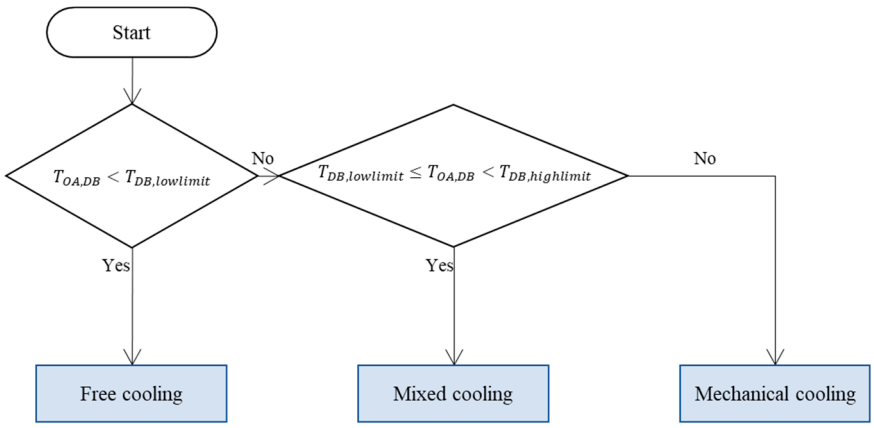

* For evaporative cooling $T_{OA,EDB}$ instead of $T_{OA,DB}$ where, $\epsilon_{EC} = \frac{T_{OA,DB} - T_{OA,EDB}}{T_{OA,DB} - T_{OA,WB}}$

$T_{OA,DB}$: Outdoor dry-bulb temp. [℃]
$T_{OA,WB}$: Outdoor wet bulb temp.[℃]
$T_{DB,lowlimit}$: Economizer low limit dry-bulb temp. [℃]
$T_{DB,highlimit}$: Economizer high limit dry-bulb temp. [℃]

(**b**)

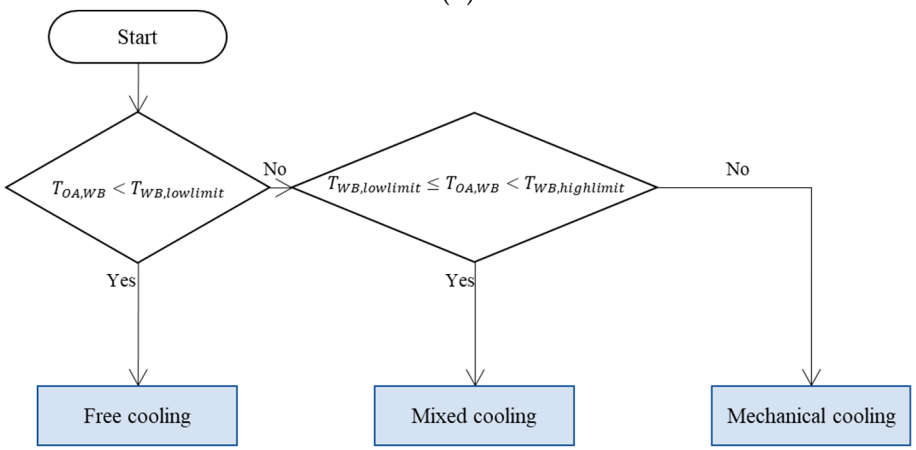

$T_{OA,WB}$: Outdoor wet bulb temp.[℃]
$T_{DB,lowlimit}$: Economizer low limit wet bulb temp. [℃]
$T_{DB,highlimit}$: Economizer high limit wet bulb temp. [℃]

(**c**)

Figure 3. Flow charts of economizer operation conditions: (**a**) DASE; (**b**) IASE; (**c**) WSE.

WSE operation depends on the outdoor wet-bulb temperature ($T_{OA,WB}$), low-limit wet-bulb temperature ($T_{WB,lowlimit}$), and high-limit wet-bulb temperature ($T_{WB,highlimit}$), as shown in Figure 3c. In the free cooling mode, if $T_{OA,WB}$ is below $T_{WB,lowlimit}$, chilled water is indirectly cooled by cooling water through the cooling tower to maintain the chilled water supply temperature set point without chiller operation. In the mixed cooling mode, when $T_{OA,WB}$ is higher than $T_{WB,lowlimit}$ but lower than $T_{WB,highlimit}$, the cooling tower fan operates at maximum speed, and the chiller maintains the chilled water supply temperature. In the mechanical cooling mode, if $T_{OA,WB}$ exceed $T_{WB,highlimit}$, chilled water and cooling water bypass the heat exchanger, and all cooling loads are managed by the chiller.

2.4. Energy Model

In this study, a thermodynamic model was developed to estimate the energy requirements of a data center cooling system. The model depicted in Figure 4 calculates the heat transfer sequentially, starting with the cooling load ($q_{cooling}(t)$) generated within the data center. This heat is then transferred through the CRAH to the cooling tower, ultimately dissipating into the atmosphere. The model determines the required flow rates of the cooling media (air and water) on an hourly basis to efficiently remove the heat generated from the data center, and the power consumption of the equipment (e.g., fans, pumps, and chillers) is derived through heat and mass transfer calculations. This process considers multiple factors, including equipment specifications and dynamic conditions (e.g., PLR and cooling medium temperatures). The model accurately assesses the cooling energy required by the data center by summing the power consumption of all of the cooling system components on an hourly basis.

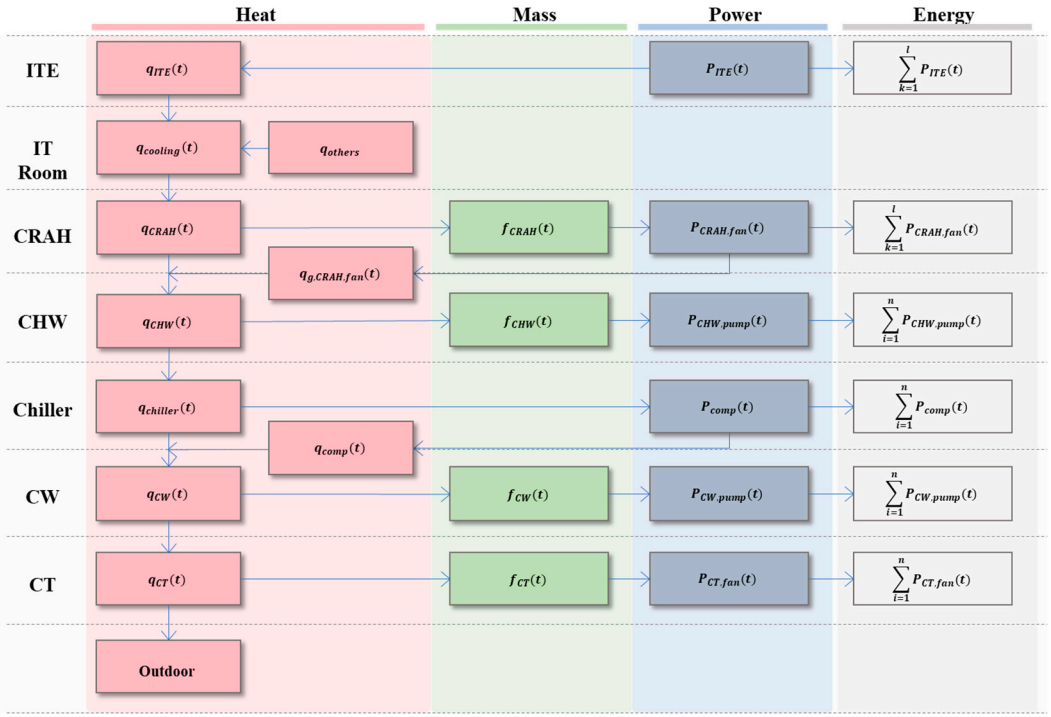

Figure 4. Diagram of heat, mass, and power flow from IT room to cooling tower (without economizer).

In the data center, the cooling load attributed to the building envelope is relatively minor compared to the overall cooling load. Furthermore, no occupant load contributes to heat generation. To simplify the calculation of the data center cooling load, the cooling load is primarily attributed to the heat produced by the ITE ($q_{ITE}(t)$), and heat is calculated by multiplying the heat generation density per rack by the total number of racks. In estimating

other cooling loads, a constant value of 0.054 kW per unit floor area was assumed, as detailed in [40], to facilitate the simplification of the calculation process.

The power consumption of each cooling system component is not only influenced by its inherent capabilities but also by varying factors, such as the PLR and cooling medium temperatures. To address these fluctuations in the equipment performance, an equipment model was developed, which incorporated the calculated PLR and cooling-medium temperature conditions, achieved through heat and mass balance calculations, as depicted in Figure 5. To ensure precise power consumption calculations for the equipment, an algorithm from the EnergyPlus program [41] was adopted. The equations for calculating heat, mass, and equipment power at each time step are presented in Appendix A.

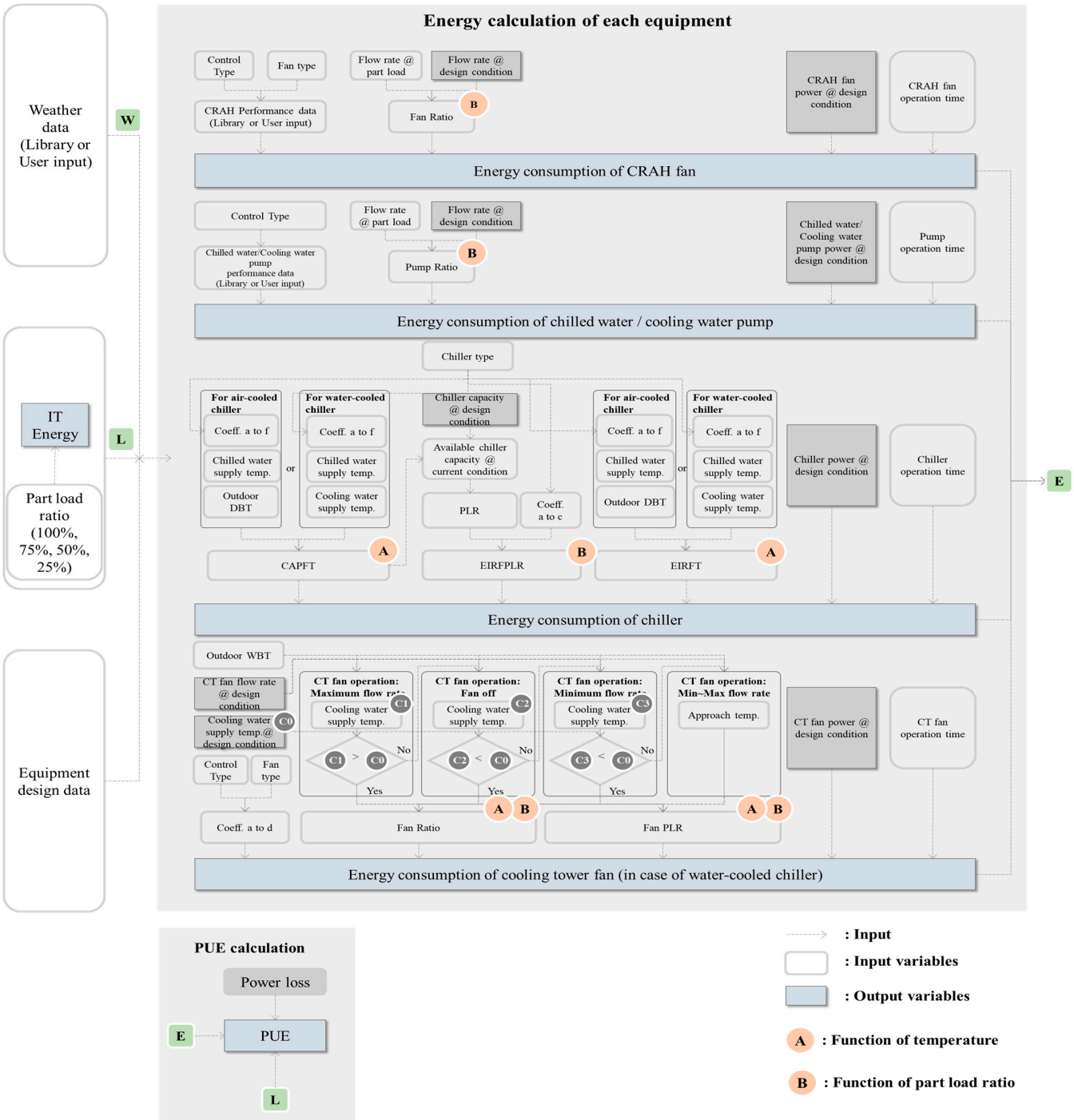

Figure 5. Flow chart of cooling energy and PUE calculation (without economizer).

The heat, mass, power, and energy flows during the free cooling mode when the economizer is incorporated into the cooling system are depicted in Figures 6–8, respectively. For both the DASE and IASE, the water loop system is not utilized during the free cooling mode; therefore, only the CRAH and EA fans are activated, as illustrated in Figures 6 and 7. In the case of the WSE, as shown in Figure 8, the chiller unit is bypassed, and the chilled water is cooled through a water-to-water heat exchanger before being released into the atmosphere via the cooling tower. The configuration of the mechanical cooling mode remains consistent with that presented in Figure 4. In the mixed cooling mode, in which both the free cooling and mechanical cooling modes operate in conjunction, the calculation flow is constructed by combining the mechanical cooling and free cooling modes.

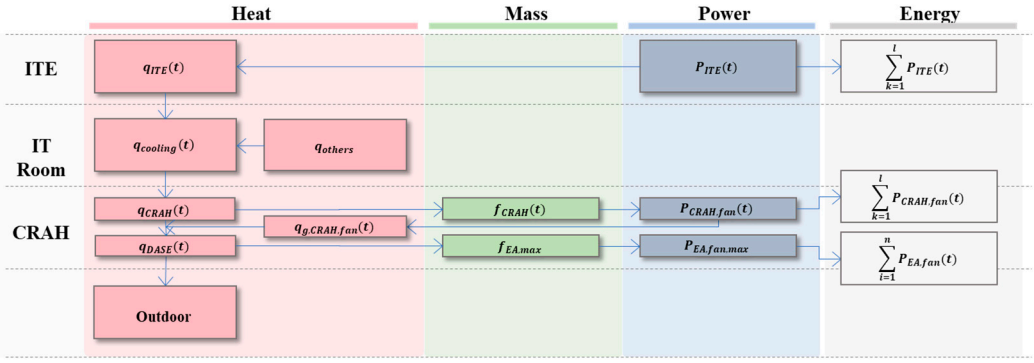

Figure 6. Diagram of heat, mass, and power flow from IT room to cooling tower (Free Cooling mode of DASE).

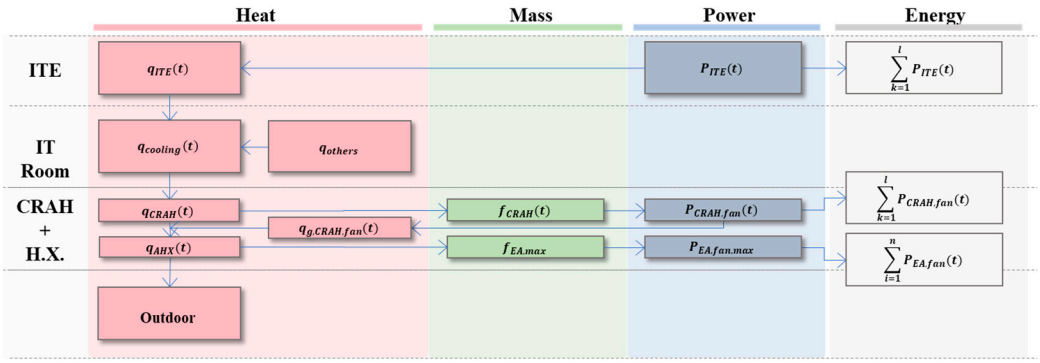

Figure 7. Diagram of heat, mass, and power flow from IT room to cooling tower (Free Cooling mode of IASE).

As previously stated, after calculating the hourly power consumption according to the economizer operation mode, the PUE of the data center was established at each time step, and the annual PUE is derived using the following equations:

$$PUE(t) = \frac{P_{ITE}(t) + P_{coolng}(t) + P_{ohters} + P_{elec,loss}(t)}{P_{ITE}(t)} \quad (1)$$

$$Annual\ PUE = \sum_{t=1}^{8760} \frac{P_{ITE}(t) + P_{coolng}(t) + P_{others} + P_{elec,loss}(t)}{P_{ITE}(t)} \quad (2)$$

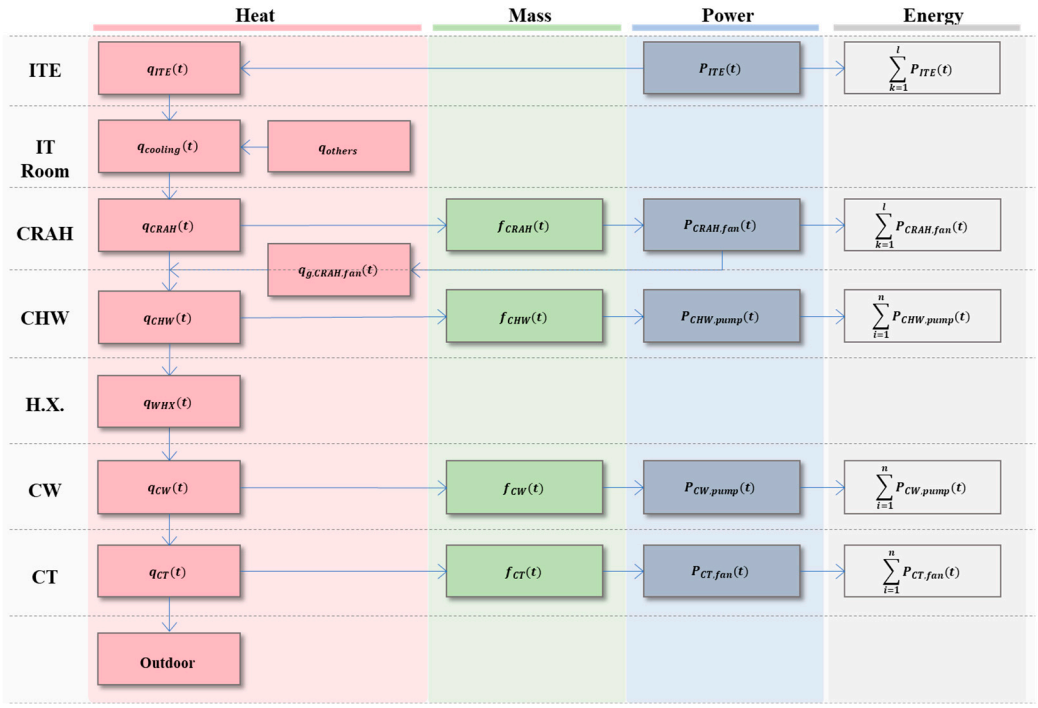

Figure 8. Diagram of heat, mass, and power flow from IT room to cooling tower (Free Cooling mode of WSE).

3. Model Verification

Validation of the developed tool (DCSim) involved a comparison with data obtained from DesignBuilder, a commercial energy analysis tool that employs the EnergyPlus algorithm. For the purpose of this validation, a data center in Incheon was modeled, predicated on the assumption of a 10 MW ITE load. To validate the energy analysis algorithm for the cooling system, the hourly cooling load results, produced by DesignBuilder, were employed as input for the DCSim. In the server room, containment was assumed to be implemented to enhance air management. The SA temperature of the CRAH was set at 2 °C lower than the temperature of the cold aisle, accounting for the heat gains from the SA to the containment.

The cooling system was based on a chilled-water system configuration. To maintain a cold aisle set temperature of 25 °C, the SA temperature from the CRAH was set to 23 °C. The temperature difference of the CRAH was determined as 12 °C, considering a temperature delta of 10 °C between the server inlet and outlet temperatures, along with an additional 2 °C for anticipated heat gains. For the chilled water system, the chilled water supply temperature was set to 10 °C, and the return water temperature to 18 °C. Additionally, the cooling water supply temperature and return water temperature were defined as 30 °C and 35 °C, respectively. To ascertain the capacity of the equipment, the autosize function in DesignBuilder was employed, and the derived values were subsequently utilized as input data for the DCSim, as presented in Table 1.

The validation process also included verification of the model with DASE implementation. In this model, an EA fan was added to the economizer to draw outdoor air. The economizer control is based on both the outdoor dew point temperature and the dry-bulb temperature, as depicted in Figure 3a. The program incorporates user-defined high and low limits for the dry-bulb temperature, as well as the ASHRAE thermal guideline's dew point temperature upper limit (15 °C). According to the control logic, if the outdoor dew point temperature is above 15 °C or the dry-bulb temperature exceeds the high limit, the Mechanical Cooling mode is activated. In the case where the outdoor dew point temperature is below 15 °C and the dry-bulb temperature falls within the high and low limits, the Mixed Cooling mode is activated. Lastly, when the outdoor dew point temperature

is below 15 °C and the dry-bulb temperature is under the user-defined low limit, the free cooling mode is initiated.

Table 1. Cooling system parameters.

Components	Parameters	Values	
		DesignBuilder	DCSim
CRAH fan	Supply temp./Return temp.	23/35 °C	23/35 °C
	Design flow rate	778.6 m^3/s	778.6 m^3/s
	Static pressure	500 Pa	-
	Rated fan power	556.1 kW	556.1 kW
Chiller	Capacity	14,537.5 kW	14,537.5 kW
	COP	8	8
	Rated power	1817.2 kW	1817.2 kW
CHW pump	Supply temp./Return temp.	10/18 °C	10/18 °C
	Design flow rate	0.432921 m^3/s	0.432921 m^3/s
	Static pressure	400,000 Pa	-
	Rated pump power	246.7 kW	246.7 kW
CW pump	Supply temp./Return temp.	30/35 °C	30/35 °C
	Design flow rate	0.7826 m^3/s	0.7826 m^3/s
	Static pressure	400,000 Pa	-
	Rated pump power	445.9 kW	445.9 kW
Cooling tower (Counter flow)	Capacity	16,258 kW	16,258 kW
	Design approach temp.	5 °C	5 °C
	Rated fan power	171.7 kW	171.7 kW
EA fan (For DASE)	Design flow rate	778.6 m^3/s	778.6 m^3/s
	Static pressure	200 Pa	-
	Rated fan power	222.4 kW	222.4 kW

The time-varying power consumption of the equipment in both the chilled water (baseline) and DASE systems is shown in Figure A2 (in Appendix B). Specifically, Figure A2a–c illustrate the hourly power consumption of the CRAH fan, chiller, and cooling tower fan in the chilled-water system, whereas Figure A2d–f show the hourly power consumption of the chiller, pump, and cooling tower fan in the DASE system. The graphs demonstrate remarkable agreement between the results obtained from DCSim and DesignBuilder. The congruence of the power consumption waveforms indicate that both programs employed identical calculation algorithms under the given input conditions. This verification confirms the successful implementation of the EnergyPlus algorithm in DCSim.

Table 2 compares the annual cooling energy and coefficient of variation of root mean square error (CVRMSE) for each piece of equipment between the baseline model and the model incorporating an economizer. The comparison was performed using DCSim and DesignBuilder. According to the ASHRAE Guideline 14 [42], a model is considered valid if the CVRMSE value is below 15% for monthly data or 30% for hourly data. In the baseline model, when calculating the CVRMSE using hourly data, the CRAH fan and chiller exhibited CVRMSE values below 2%, the cooling water and chilled-water pumps displayed CVRMSE values of 0%, and the cooling tower fan demonstrated 9.3%, respectively. Although the CVRMSE values of the cooling tower fan were relatively higher CVRMSE than those of the other equipment, the values remained significantly lower than the validity threshold of 30%. In the model with the applied economizer, the hourly data-based CVRMSE results were as follows: CRAH fan (1.4%) chiller, (10.2%); cooling water and chilled-water pumps (4.8%); and cooling tower fan (10.75%). All values met the validity criteria, indicating a good agreement between DCSim and DesignBuilder for the model with the economizer.

Table 2. Comparison of cooling energy and CVRMSE.

Equipment	Chilled Water System			Chilled Water System + DASE		
	Energy Consumption MWh		CVRMSE %	Energy Consumption MWh		CVRMSE %
	DesignBuiler	DCSim		DesignBuiler	DCSim	
CRAH fan	3776	3732	1.16	3704	3732	1.40
Chiller	10,362	10,160	1.96	3106	3005	10.24
CHW pump	2127	2127	0.00	687	687	4.75
CW pump	3844	3844	0.00	1242	1243	4.75
CT fan	168	178	9.29	108	111	10.70

4. Results and Discussion

Utilizing the previously validated economizer system, DCSim was employed to carry out a climate-zone-specific comparison of economizer performance. The objective was to identify the most advantageous air-side economizer strategy for minimizing cooling energy consumption and enhancing the PUE across different climate zones. Additionally, a sensitivity analysis was conducted to pinpoint the primary factors influencing PUE, particularly focusing on the temperature conditions of the cooling medium. This analysis also included an assessment of the uncertainty in PUE values specific to each climate zone, attributable to variations in these influential factors.

4.1. Comparison of Economizer Performance by Climate Zone

To compare the performances of the economizer systems across various climate zones, Asian cities were selected to correspond to each ASHRAE climate zone [38], as detailed in Table 3. The hourly cooling energy consumption and PUE were calculated using Typical Meteorological Year (TMY) weather data [43] for each chosen city. The equipment parameters required for the simulations were established based on the values used in the validation simulations. In addition, to model IASE and EC, the air-to-air heat exchanger effectiveness and EC effectiveness were set to 0.7 and 0.6, respectively, based on EnergyPlus engineering reference [41].

Table 3. Selected climate zones and cities in Asia.

Climate Zone WMO#	Description	Annual Average Values		Representative City
		Temperature °C	Relative Humidity %	
0A/484560	Extremely hot and wet	28.5	71.0	Bangkok, Thailand
0B/412160	Extremely hot and dry	27.1	60.6	Abu Dhabi, United Arab Emirates
1A/488200	Very hot and wet	23.9	79.9	Hanoi, Vietnam
1B/405820	Very hot and dry	26.5	39.0	Kuwait Intl Airport, Kuwait
2A/466960	hot and wet	22.8	80.9	Taipei, Taiwan
3A/574940	Warm and wet	17.3	75.7	Wuhan, China
3B/407540	Warm and dry	17.3	40.6	Tehran Mehrabad, Iran
4A/471120	Mixed humid	11.9	68.8	Incheon, Korea
4B/407060	Mixed and dry	12.0	53.5	Tabriz, Iran
5A/474120	Cool and wet	8.8	69.1	Sapporo, Japan
5B/516280	Cool and dry	10.0	45.9	Xinjiang Uygur, China
6A/541610	Cold and wet	5.5	65.4	Changchun, China
6B/534630	Cold and dry	6.6	52.9	Hohhot, China
7/361770	Very cold	4.3	64.9	Semipalatinsk, Kazakhstan
8/307580	Subarctic/Arctic	−0.8	67.9	Chita, Russia

Table 4 presents the annual percentage of operating hours by mode for each ASHRAE climate zone based on air-side economizer type. In the case of the DASE system, the 0A zone would predominantly utilize the mechanical cooling mode for over 96% of its operating hours, indicating limited benefits from implementing the DASE system. However, in climate zones from 3B onwards, over 50% of the operating hours could be allocated to the free cooling mode, highlighting the significant positive impact of the DASE system. Within climate zones ranging from 0A to 4B, the dry zones (0B, 1B, 3B, and 4B) exhibited higher percentages of operating hours under the free cooling mode and considerably lower percentages under the mechanical cooling mode than the wet zones (0A, 1A, 2A, 3A, and 4A) when utilizing the DASE system. The performance of the DASE system is influenced by outdoor humidity levels. In wet zones, despite the suitable outdoor temperature conditions for cooling, high humidity can restrict the feasibility of outdoor cooling; therefore, implementing DASE in dry zones is more suitable than in wet zones within climate zones 0A to 4B. In climate zones 5A and beyond, the dew point temperature typically remains below 15 °C, even in wet zones where relative humidity is high; therefore, the distinction between the dry and wet zones in terms of free cooling mode duration becomes less pronounced. When EC was introduced into the DASE system (DASE + EC), the dry zones exhibited a significant increase in the free cooling mode duration, ranging from 10.6% to 55.5% across the different climate zones. However, in wet zones, the addition of EC did not result in a substantial difference in the duration of free cooling.

The IASE system is unaffected by outdoor humidity conditions, and only a minor difference was observed in the operating mode durations between the dry and wet zones. Nevertheless, it was noted that from 0A zone to 1B zone, longer free cooling durations occurred in the dry zones than in the wet zones. However, these dry zones also experienced increased instances of mechanical cooling. Zones with higher temperatures and lower humidity tend to experience larger temperature fluctuations between day and night because of the limited moisture content in the air, resulting in a reduced thermal capacity of the air. Consequently, increased opportunities exist for free cooling during the nighttime in zones such as 0B and 1B, which are characterized by hot and dry conditions; however, rising temperatures occur during the daytime and the number of mechanical cooling hours subsequently increase. With the integration of the EC into the IASE system (IASE + EC), the duration of the free cooling mode increased across all climate zones owing to the supplementary effect of EC. Notably, the increase in the free cooling mode duration resulting from the addition of EC was more significantly pronounced in the dry than in the wet zone.

The distribution of the hourly PUE based on the air-side economizer type for each climate zone is shown in Figure 9. As the proportion of mechanical cooling increased, a higher frequency of PUE values of approximately 1.4 was observed, which resulted in enlargement of the upper area of the graph. Similarly, a greater occurrence of mixed cooling corresponded to a larger middle area, whereas a higher proportion of Free Cooling resulted in an increased frequency of PUE values of approximately 1.2, contributing to the expansion of the lower area of the graph.

The graph illustrating the 0A zone (Figure 9a) shows that both the DASE and DASE + EC systems are primarily operating in the mechanical cooling mode. However, the IASE and IASE + EC systems show increasing mixed cooling mode operation occurrences. This phenomenon implies that for the 0A zone, implementing the IASE system might offer more substantial PUE reduction benefits than implementing the DASE system. When examining the graphs for 0B and 1A zones, introducing the IASE system increases mixed cooling and free cooling occurrences, which reduces the annual PUE by 0.03 to 0.06 compared with that in the DASE system. In the 1B zone, the PUE distribution between the DASE and IASE systems is similar, and the addition of EC significantly decreases the frequency of operation at the upper PUE limit because of the dry climate conditions. For zones 2A and 3A, which are characterized by higher humidity levels, the implementation of IASE instead of DASE reduces the frequency of operation at the upper PUE limit, and the impact of adding EC is not significant. In climate zones 3B and beyond, where the free-cooling

operation exceeded 50% of the year, the shape of the graph changes, and the lower area becomes more prominent than the upper area. In zones 3B, 4B, and 5B, distinguishing between the PUE distributions of the DASE and IASE is challenging, but the addition of EC to these dry climate zones significantly concentrates the PUE distribution toward the lower end. In the 4A, 5A, and 6A climate zones, the IASE system displays a more concentrated PUE distribution toward the lower end than the DASE system, and the impact of EC on the hourly PUE distribution is negligible. Finally, in climate zones 6B, 7, and 8, the distribution of PUE values is similar across different systems, and all systems exhibit a concentrated distribution of PUE values toward the lower end. This finding implies a significant economizer effect, irrespective of the specific system type.

Table 5 provides data comparing the relative annual cooling energy consumption between different air-side economizers for each climate zone. The energy usage of a system without economizer implementation (referred to as the Baseline) was set at 100%, and cooling energy levels for different economizer types were then compared to this baseline. In both the 0A and 0B zones, the application of IASE + EC proved to be more effective in reducing cooling energy consumption compared with that in other systems. In the wet zones, both IASE and IASE + EC demonstrated advantages for cooling energy reduction, whereas in dry zones, the addition of EC yielded greater cooling energy savings. This observation aligns with the findings from the earlier analysis of economizer operating hours and the hourly PUE distribution. For zones 7 and 8, implementing economizers resulted in a cooling energy consumption reduction of approximately 60–70% across all system types. Notably, in the case of the IASE + EC scenario for climate zone 8, where 8759 out of the total 8760 h operated exclusively in the free cooling mode (as referenced in Table 4), the projected annual cooling energy consumption was estimated as 30% of the baseline. This observation implies that the energy used by the CRAH fan and exhaust fan constituted roughly 30% of the baseline energy consumption. Therefore, achieving an annual cooling energy reduction of 30% or less through economizer application would require additional measures to curtail fan energy consumption.

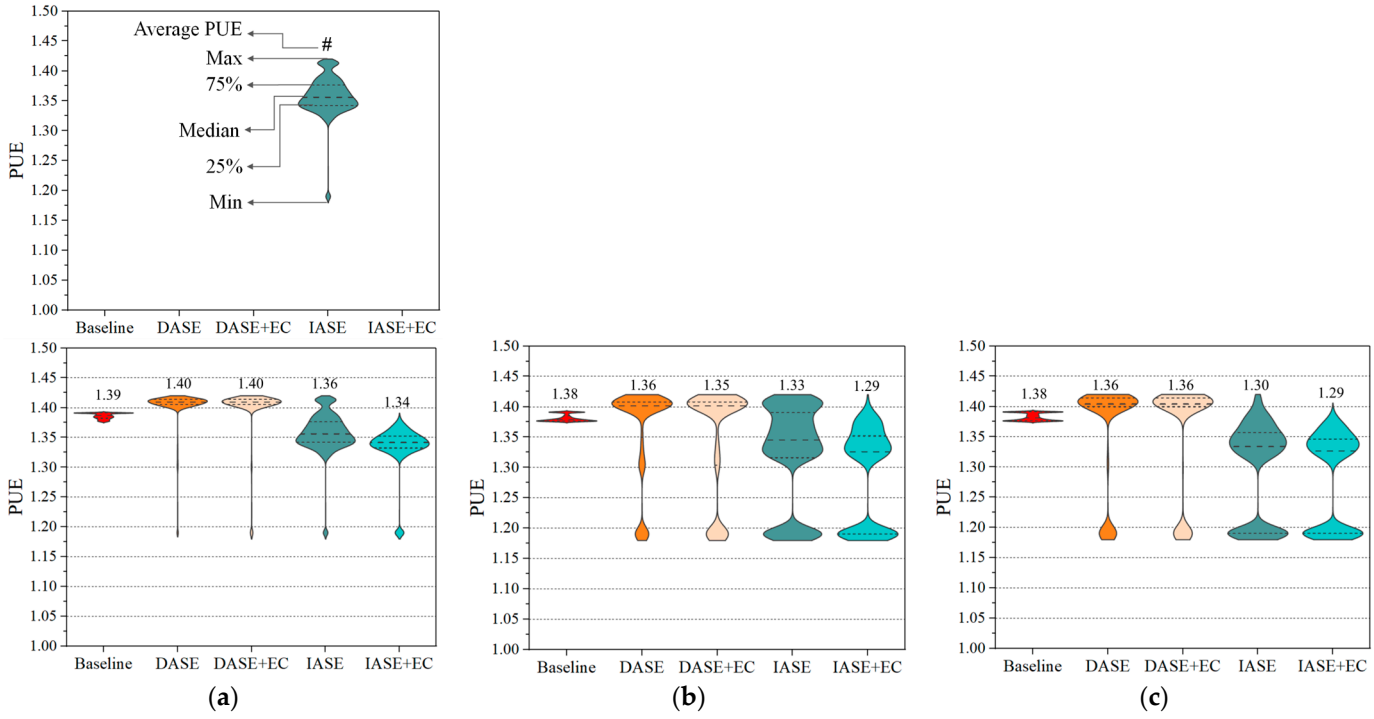

Figure 9. *Cont.*

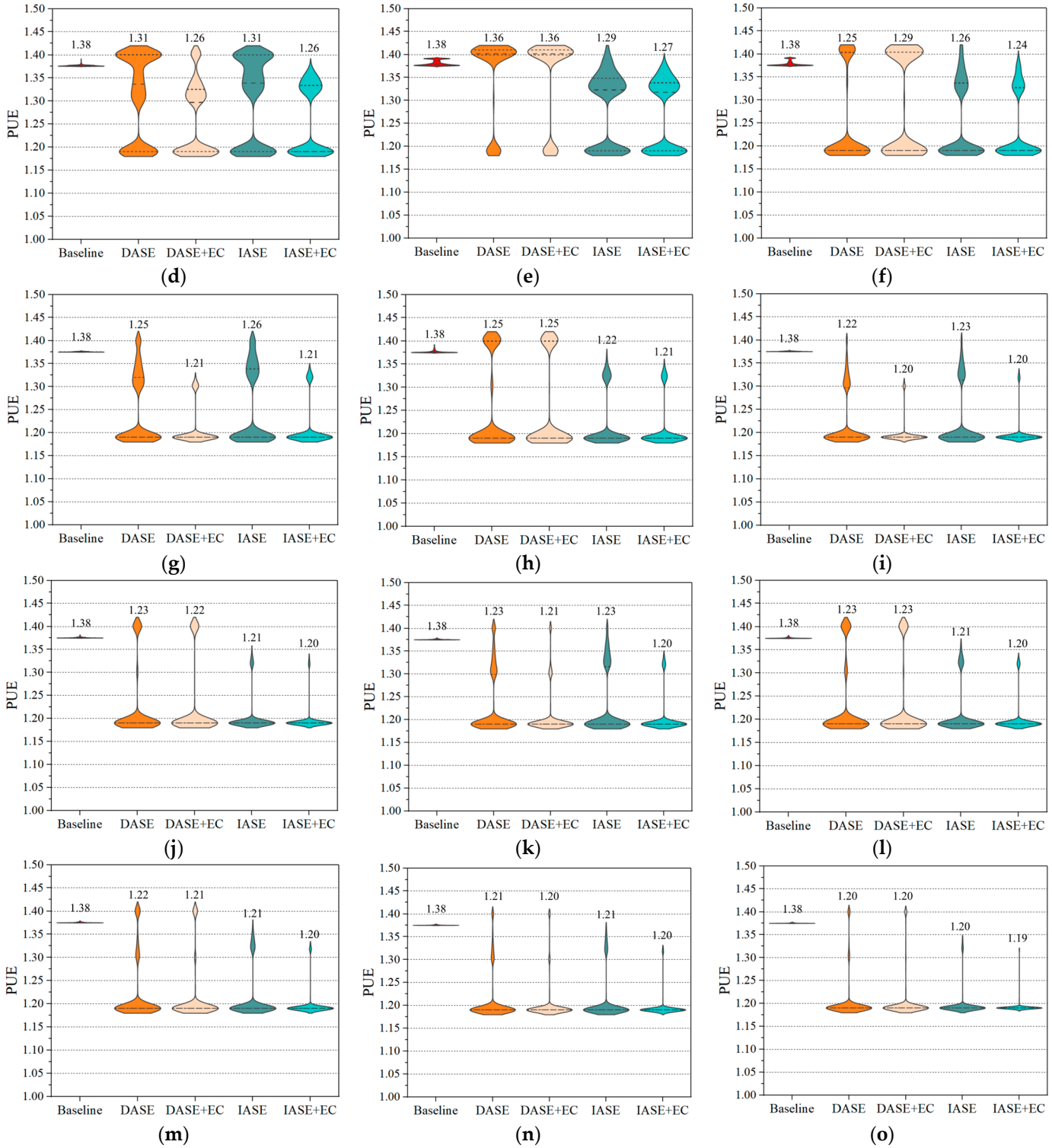

Figure 9. Hourly PUE according to climate zone and air-side economizer type: (**a**) 0A zone; (**b**) 0B zone; (**c**) 1A zone; (**d**) 1B zone; (**e**) 2A zone; (**f**) 3A zone; (**g**) 3B zone; (**h**) 4A zone; (**i**) 4B zone; (**j**) 5A zone; (**k**) 5B zone; (**l**) 6A zone; (**m**) 6B zone; (**n**) 7 zone; (**o**) 8 zone.

Table 4. Percentage of operating hours by mode.

Climate Zone	DASE			DASE + EC			IASE			IASE + EC		
	Free Cooling	Mixed Cooling	Mechanical Cooling	Free Cooling	Mixed Cooling	Mechanical Cooling	Free Cooling	Mixed Cooling	Mechanical Cooling	Free Cooling	Mixed Cooling	Mechanical Cooling
0A	1	3	96	3	1	96	2	90	9	5	95	0
0B	15	12	73	23	10	68	22	57	22	36	64	0
1A	20	2	77	22	1	77	31	67	2	37	63	0
1B	33	28	39	49	40	11	35	35	30	53	47	0
2A	22	1	77	23	0	77	36	63	2	44	56	0
3A	72	2	26	53	1	47	59	37	3	65	35	0
3B	59	34	6	84	16	0	59	35	6	84	16	0
4A	69	3	28	72	0	28	77	23	0	83	17	0
4B	75	24	2	94	6	0	75	24	1	94	6	0
5A	82	2	16	84	0	16	89	11	0	95	5	0
5B	73	22	5	88	9	3	73	25	2	89	11	0
6A	78	6	16	83	1	16	83	17	0	91	9	0
6B	80	11	9	89	3	9	84	16	0	94	6	0
7	85	12	3	94	3	3	87	13	0	96	4	0
8	91	4	4	95	1	4	94	6	0	99	1	0

Table 5. Comparison of relative annual cooling energy consumption among different air-side economizer types and climate zones.

Climate Zone	Relative Annual Cooling Energy Consumption				
	Baseline	**DASE**	**DASE + EC**	**IASE**	**IASE + EC**
0A	100%	106%	106%	90%	82%
0B	100%	94%	88%	80%	67%
1A	100%	92%	91%	70%	65%
1B	100%	76%	58%	74%	56%
2A	100%	91%	91%	66%	60%
3A	100%	53%	67%	54%	50%
3B	100%	53%	37%	55%	38%
4A	100%	54%	52%	42%	39%
4B	100%	43%	33%	45%	33%
5A	100%	44%	43%	36%	33%
5B	100%	45%	37%	46%	36%
6A	100%	46%	44%	39%	35%
6B	100%	42%	38%	39%	33%
7	100%	38%	34%	38%	32%
8	100%	36%	34%	33%	31%

4.2. Sensitivity and Uncertainty Analysis of Cooling Medium Temperature on PUE

A two-level factorial design was employed to identify the significant factors associated with the cooling medium temperature conditions on PUE. A factorial design is a useful approach when multiple factors influence outcomes, enabling an examination of the significance of each factor and the exclusion of less influential factors. The factors considered for the impact analysis included the CRAH supply temperature, CRAH temperature difference, chilled water supply temperature, chilled water temperature difference, cooling water supply temperature, and cooling water temperature difference. The two-level values for these factors were determined based on the literature [28,35,44–46] and are outlined in Table 6.

Table 6. Level of factors influencing annual PUE.

Factors	Low °C	High °C
CRAH supply temperature	13	30
CRAH temperature difference	10	15
Chilled water supply temperature	7	18
Chilled water temperature difference	5	10
Cooling water supply temperature	30	35
Cooling water temperature difference	5	8

To assess the impact of these six factors on the annual PUE, a full factorial design was executed, resulting in 64 (2^6) simulations for each economizer system strategy. Other system parameters (excluding these six factors) were set using data from the hourly PUE analysis, and weather data from the 4A climate zone were applied in the simulations.

The results of the sensitivity analysis, as depicted in Figure 10, revealed that among the cooling medium temperature settings, the CRAH supply temperature and CRAH temperature difference had a significant impact on the annual PUE. Specifically, for the DASE and DASE + EC systems, the CRAH temperature difference emerged as the dominant factor, followed by the CRAH supply temperature. In contrast, for the IASE and IASE + EC systems, the CRAH supply temperature was the primary influencer, with the CRAH temperature difference exerting the second-most significant effect. The CRAH supply temperature was closely associated with the operation time of the free-cooling mode, as higher CRAH supply temperatures lead to increased utilization of free cooling. However, for DASE or DASE + EC systems, the impact of the CRAH supply temperature was

diminished due to humidity constraints (dew point temperature of 15 °C) that restricted the expansion of the Free Cooling mode operation, even when the CRAH supply temperatures were higher. Conversely, as the IASE approach lacks humidity restrictions during the free-cooling operation, the CRAH supply temperature played a more prominent role in influencing the PUE.

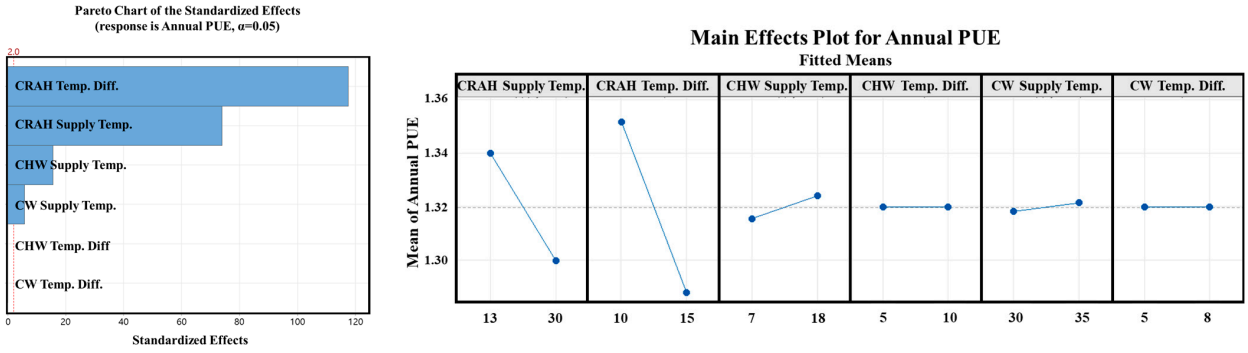

(**a**)

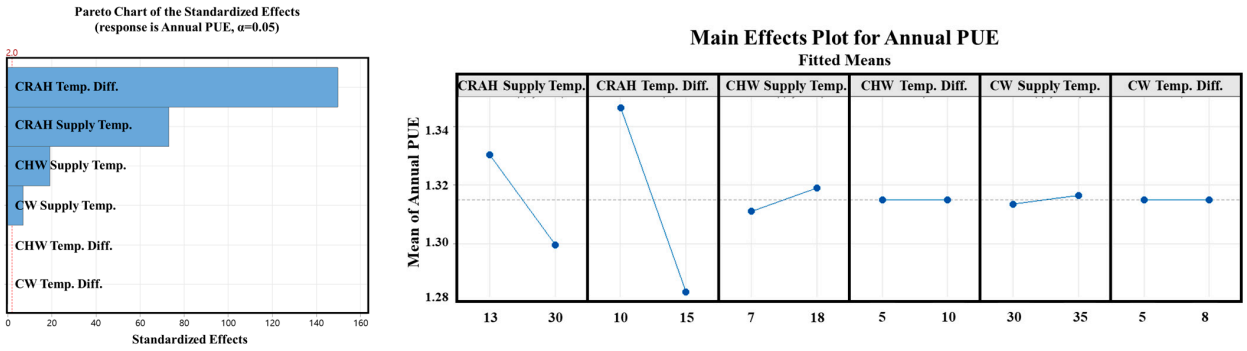

(**b**)

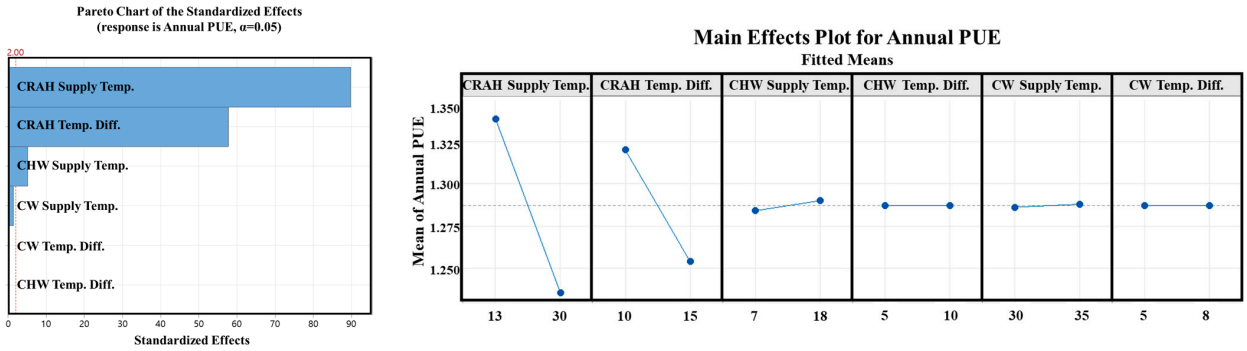

(**c**)

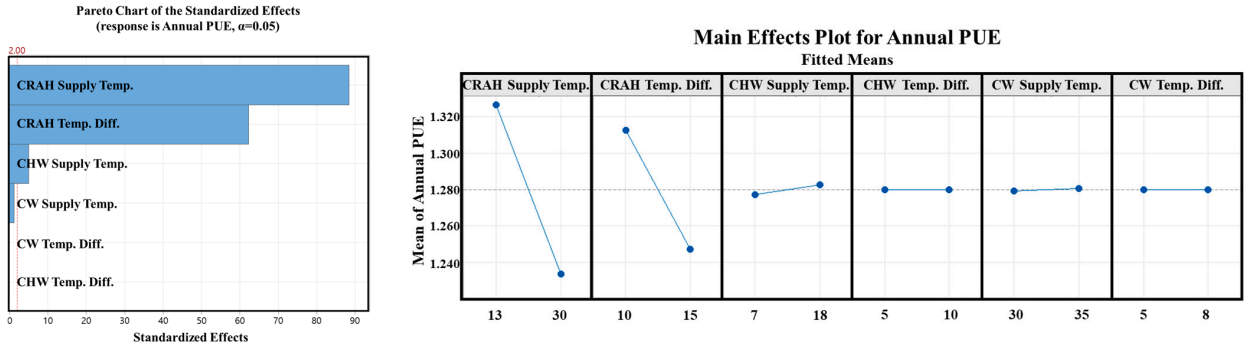

(**d**)

Figure 10. Pareto charts and factorial plots for annual PUE using economizers (DASE/IASE/WSE): (**a**) DASE; (**b**) DASE + EC; (**c**) IASE; (**d**) IASE + EC.

An uncertainty analysis of the average PUE across different climate zones was conducted for each economizer system, focusing on the CRAH supply temperature and the CRAH temperature difference, which had a significant impact on the annual PUE through the results of the sensitivity analysis. The ranges between the low and high values of these two factors, as outlined in Table 6, were divided into ten intervals each. By incorporating input values from the previous hourly PUE analysis, 121 cases were generated for each economizer system, consisting of 11 cases for the CRAH supply temperature and 11 cases for the CRAH temperature difference. The uncertainties in the average PUE resulting from variations in these two factors across various climate zones for each economizer strategy are shown in Figure 11, which also displays the mean, median, percentiles (25th − 1.5 × IQR, 25th, 75th, and 75th + 1.5 × IQR) of the predicted PUE distributions obtained from the model.

For the DASE and DASE + EC systems, the PUE values of dry zones (1B, 3B, and 4B) exhibited a broader range of uncertainties than those in wet zones (1A, 2A, 3A, and 4A). Notably, this range extended further towards lower values, indicating a greater potential for reducing the PUE in dry zones by adjusting these two factors. For the IASE system, the differences in the PUE uncertainty between the dry and wet zones appeared to be similar. However, for climate zones 0A, 0B, 1A, 1B, and 2A, greater uncertainty was observed compared with that in the other zones, suggesting that variations in the CRAH supply temperature and the CRAH temperature difference have a more significant impact on the PUE in these regions. Consequently, careful consideration should be given to the design of these two factors when implementing IASE or IASE + EC systems in these zones. From region 6A onwards, the uncertainty in the annual PUE was similar across different economizer types. Adjusting the two influencing factors was estimated to lead to a further reduction in the PUE by approximately 0.08 to 0.12 in these zones.

Given the impact of variables such as ITE load, outdoor and indoor environmental conditions, and equipment efficiency on PUE, there exists an inherent limitation in directly comparing the outcomes of this study with those of previous research conducted under different conditions. Nonetheless, a review of existing studies analyzing PUE values has revealed, as detailed in Table 7, that PUE displays a distribution ranging from 1.05 to 1.90 across various climate zones and CRAH SAT settings. This range is observed to include the PUE spectrum of 1.16 to 1.43 identified in the current research.

Table 7. PUE range of previous studies.

Economizer Type	References	Climate Zones	CRAH SAT °C	PUE
DASE	[15]	17 Climate zones	23~27	1.37~1.42
	[29]	19 Climate zones	15	1.31~1.48
	[33]	0A, 0B, 4A, 7 zones	22	1.35~1.90
	[34]	4A zone	16~22	1.50~1.62
	[35]	17 cities	NA	1.05~1.80
	[36]	2A,4A,7 zones	NA	1.38~1.43
	[37]	925 locations	NA	1.33~1.48
DASE + EC	[33]	0A, 0B, 4A, 7 zones	22	1.34~1.90
	[34]	4A zone	16~22	1.48~1.63
IASE	[29]	19 Climate zones	15	1.31~1.48
	[33]	0A, 0B, 4A, 7 zones	22	1.32~1.86
	[34]	4A zone	16~22	1.54~1.66
IASE + EC	[29]	19 Climate zones	15	1.30~1.48

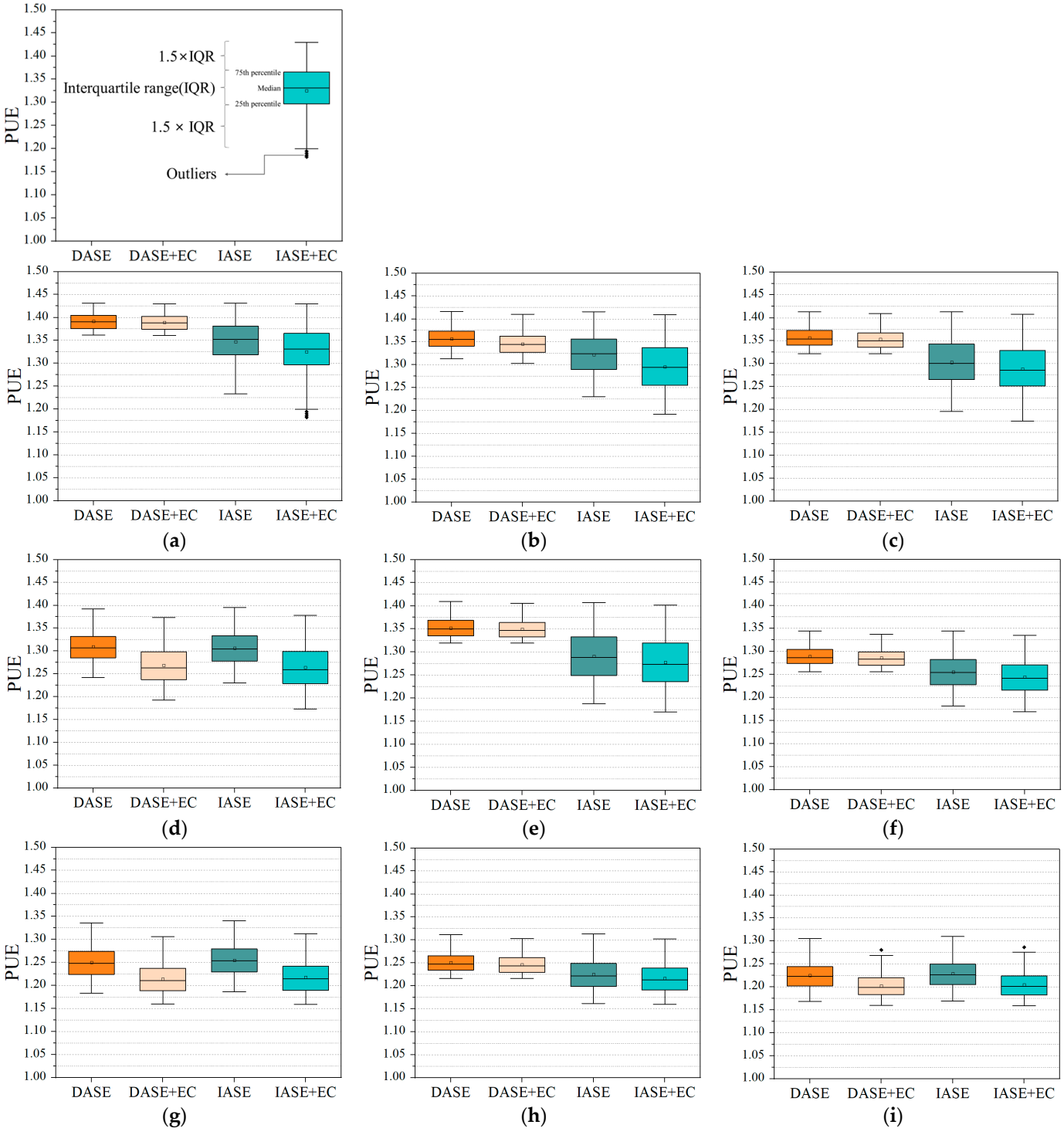

Figure 11. *Cont.*

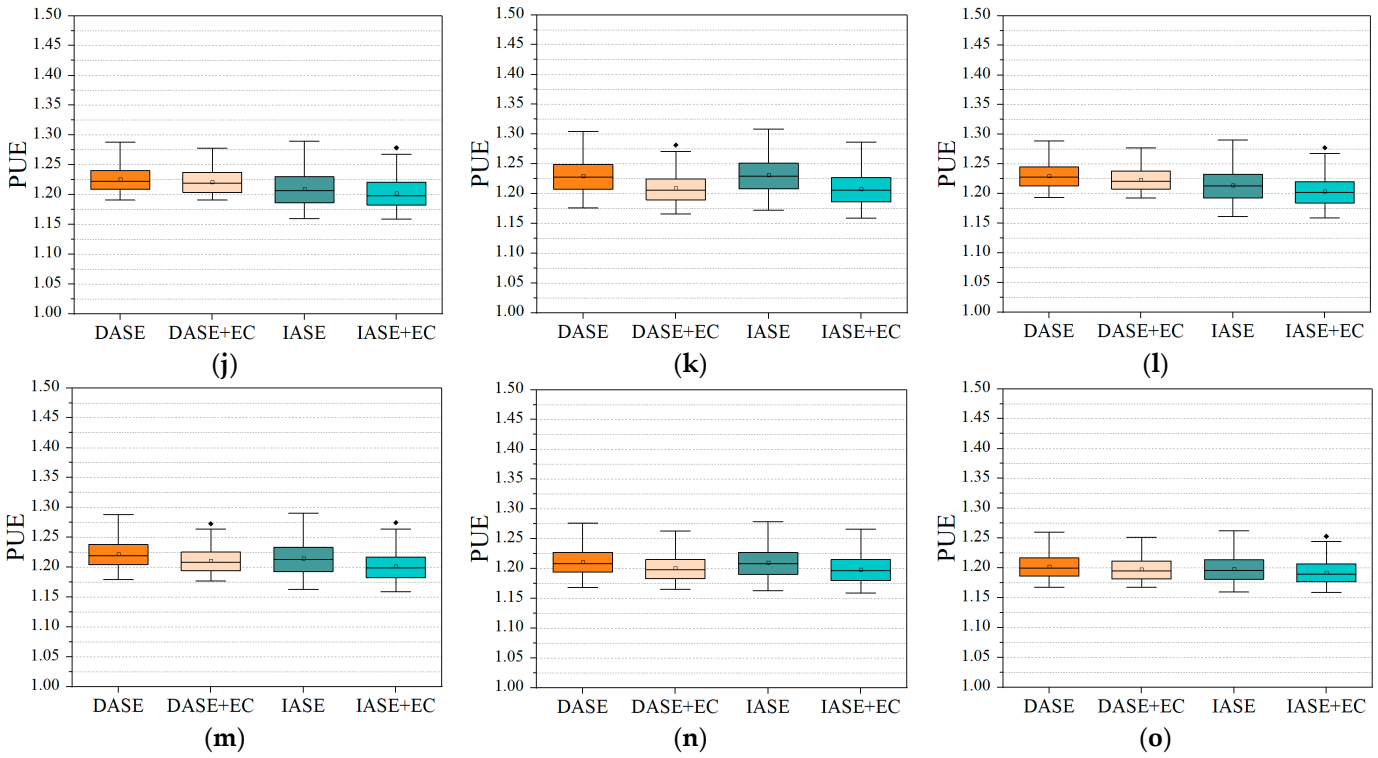

Figure 11. Uncertainties in average PUE according to climate zone and air-side economizer type: (**a**) 0A zone; (**b**) 0B zone; (**c**) 1A zone; (**d**) 1B zone; (**e**) 2A zone; (**f**) 3A zone; (**g**) 3B zone; (**h**) 4A zone; (**i**) 4B zone; (**j**) 5A zone; (**k**) 5B zone; (**l**) 6A zone; (**m**) 6B zone; (**n**) 7 zone; (**o**) 8 zone.

Limitation of the work include:

- The developed program is predominantly designed for calculating the PUE of air-cooled data centers, where servers are cooled using air supplied by CRAH. However, this approach has limitations when applied to data centers employing liquid cooling methods, such as rear-door heat exchangers.
- Through comparative analysis of data center PUE, assistance in selecting alternatives to reduce PUE can contribute to diminishing the environmental impact of data centers. However, a comprehensive evaluation of a data center's environmental impact requires consideration of multiple factors, including water usage, waste heat utilization, and the application of renewable energy sources. Therefore, further works include expanding functionalities beyond PUE analysis to encompass a more multifaceted analysis of environmental impacts, such as carbon usage effectiveness (CUE), water usage effectiveness (WUE), and energy reuse factor (ERF).
- The current program enables the relative comparison of energy usage in data centers through PUE analysis. However, to calculate the overall operational costs, considerations such as water usage and system management expenses are necessary. For a comprehensive cost analysis, additional factors such as system capital investment and benefits derived from waste heat utilization must also be taken into account. These aspects, however, exceed the scope of this research.

5. Conclusions

The primary aims of this research were to develop a tool to assist in selecting energy-efficient alternatives during the design phase of data centers and to validate the performance of this tool. The developed tool, known as DCSim, was employed to conduct a thorough PUE assessment by analyzing the impact of data center cooling system configurations and equipment parameters under various weather conditions during the early design stage. In this study, PUE distributions were compared for various economizer systems

across 14 cities categorized by ASHRAE climate zones. A sensitivity analysis was then conducted to assess the influence of six factors related to the cooling medium temperature on the annual PUE to identify factors that had the most pronounced impact on the annual PUE. Subsequently, by manipulating these factors, this study analyzed the uncertainty in the annual PUE for different climate zones and economizer systems. The key outcomes of this study are summarized as follows:

(1) Development of DCSim: The DCSim tool was developed as a dynamic energy calculation tool tailored for use in data centers. It employs the EnergyPlus algorithm to dynamically compute cooling energy, which enables adaptation to changing outdoor conditions and system parameters, particularly when economizer systems are involved.

(2) Validation of DCSim: The accuracy of the DCSim tool was verified by comparing it with DesignBuilder v7.0.2.4, a commercial building energy analysis software based on EnergyPlus. The hourly power data for each piece of equipment calculated using both tools were compared. The CVRMSE ranged from 0% to 9.3% for the baseline, and from 1.4% to 10.75% for the air-side economizer. The results showed that CVRMSE values were within the ASHRAE criteria, and the accuracy of using the DCSim compared with that in the established program was confirmed.

(3) Comparison of PUE: Using the validated DCSim tool, an extensive comparison of the PUE distributions was conducted across various ASHRAE climate zones and economizer systems. The application of IASE or IASE + EC in zones 0A and 0B showed potential annual PUE reductions of about 0.04 to 0.07 compared to DASE or DASE + EC. In dry zones, the addition of EC further enhanced cooling efficiency, resulting in PUE reductions of approximately 0.02 to 0.05, particularly in zones 1B, 3B, and 4B. Wet zones demonstrated noteworthy PUE reductions of approximately 0.03 to 0.07 with IASE implementation compared with that in DASE.

(4) Sensitivity Analysis: A sensitivity analysis was conducted using a two-level factorial design method to evaluate the impact of six cooling medium temperature-related factors on the annual PUE. The analysis revealed that the CRAH supply temperature and CRAH temperature difference were the most influential factors affecting the annual PUE. In particular, for the DASE and DASE + EC systems, the CRAH temperature difference exhibited the greatest influence, whereas for the IASE and IASE + EC systems, the CRAH supply temperature played a more dominant role in impacting the annual PUE.

(5) Uncertainty Analysis: A detailed examination of the annual PUE uncertainty was conducted, with a focus on the variations in the CRAH supply temperature and CRAH temperature difference across a variety of climate zones and system types. In the implementation of DASE and DASE + EC systems, it was observed that the upper limits of PUE in both Dry zones (0B, 1B, 3B, 4B, 5B) and Wet zones (0A, 1A, 3A, 4A, 5A) exhibited similarities. However, a significant reduction in the lower limit of PUE, ranging from approximately 0.05 to 0.13, was identified in Dry zones. In contrast, the deployment of DASE (+EC) and IASE (+EC) systems in Wet zones (0A, 1A, 2A, 3A, 4A, 5A, 6A) and region 0B showed that while the upper limits of PUE remained comparable, the application of IASE (+EC) indicated a potential reduction in the lower limit by about 0.03 to 0.18. Consequently, an elevated level of uncertainty was observed in the application of DASE and DASE + EC systems in Dry zones, and a similar pattern of uncertainty was notable for IASE and IASE + EC systems in Wet zones and region 0B. This greater uncertainty suggested that variations in CRAH supply temperature and CRAH temperature difference had a more substantial impact on PUE. Therefore, meticulous consideration of these factors is particularly crucial during system design in regions characterized by high uncertainty.

Author Contributions: Conceptualization, J.H.K., H.K. and D.U.S.; methodology, J.H.K. and H.K.; software, J.H.K. and H.K.; validation, J.H.K. and H.K.; formal analysis, D.U.S.; writing—original draft preparation, J.H.K.; writing—review and editing, J.H.K.; visualization, J.H.K. and H.K.; supervision, J.H.K. All authors have read and agreed to the published version of the manuscript.

Funding: This work was supported by the National Research Foundation of Korea (NRF) grant, funded by the Korean government (MSIT) (No. 2021R1G1A1094364), and the present research was supported by the research grant from Kwangwoon University in 2023 (No. 2023-0115).

Data Availability Statement: The raw data supporting the conclusions of this article will be made available by the authors on request.

Acknowledgments: The authors acknowledge financial support provided by POSCO E&C.

Conflicts of Interest: Author Heegang Kim was employed by the company Plant Research Group, Posco E&C. The remaining authors declare that the research was conducted in the absence of any commercial or financial relationships that could be construed as a potential conflict of interest.

Nomenclature

q	Load or heat [kW]
N	Number of items
LR	Load ratio
A	Datacenter floor area [m^2]
f	Flow rate [m^3/s]
c_p	Specific heat [kJ/kg°C]
T	Temperature [°C]
ΔT	Temperature difference [°C]
$Frac_{freeconv}$	Fraction of tower capacity in free convection regime
FR or PR	Ratio of flowrate at part load to full load flowrate
PLR	Part load ratio of chiller
FPR	Airflow rate ratio of cooling tower fan
P	Power [kW]
Y	Function of the YorkCalc
a *to* f	Correlation coefficients
Greek symbols	
ρ	Density [kg/m^3]
ϵ	Effectiveness
β	Correlation coefficients
Subscripts	
IT	ITE
$rack$	Rack
$others$	Others
$cooling$	Cooling
$chiller$	Chiller
$avail$	Available
d	Design
g	Generated
fan	Fan
$pump$	Pump
$comp$	Compressor
$fanOFF$	the cooling tower fan is in the off state
$fanMIN$	the cooling tower fan is operated at minimum speed
$fanMAX$	the cooling tower fan is operated at maximum speed

Abbreviations	
ITE	Information technology equipment
PUE	Power usage effectiveness
EC	Evaporative cooling
IASE	Indirect air side economizers
CRAH	Computer room air handler
DASE	Direct air side economizers
IEA	International energy agency
WSE	water-side economizer
PLR	part load ratio
OA	outside air
RA	return air
SA	supply air
EA	Exhaust air
WB	Wet bulb
DB	Dry bulb
DPT	Dew point temperature
CVRMSE	Coefficient of variation of root mean square error
TMY	Typical meteorological year
ASHRAE	American society of heating, refrigerating and air-conditioning engineers
a	Air
min	Minimum
w	Water
CHW	Chilled water
CW	Cooling water
CT	Cooling tower
C	Cool
H	Hot
$approach$	Cooling tower approach
$range$	Cooling tower range
OWB	Outdoor wet-bulb
ODB	Outdoor dry-bulb
AHX	Air-to-air heat exchanger
WHX	Water-to-water heat exchanger

Appendix A

Appendix A.1. Load Model

$$q_{IT}(t) = q_{rack} \times N_{rack} \times LR(t) \quad \text{(A1)}$$

$$q_{others} = 0.54 \times A \tag{A2}$$

$$q_{cooling}(t) = q_{IT}(t) + q_{others} \tag{A3}$$

Appendix A.2. Baseline Model: Chilled Water System

Appendix A.2.1. Air Loop (CRAH)

$$q_{CRAH}(t) = q_{cooling}(t) \tag{A4}$$

$$f_{CRAH,\,fan}(t) = \frac{q_{CRAH}(t)}{\rho_a c_{p,a} \Delta T_{CRAH}} \tag{A5}$$

$$FR_{CRAH}(t) = \frac{f_{CRAH,\,fan}(t)}{f_{d,\,CRAH\ fan}} \tag{A6}$$

$$P_{CRAH,fan}(t) = P_{d,CRAH\ fan} \times \left(a + b{\cdot}FR_{CRAH}(t) + c{\cdot}FR_{CRAH}(t)^2 + d{\cdot}FR_{CRAH}(t)^3\right) \tag{A7}$$

Appendix A.2.2. Chilled Water Loop (Chilled Water Pump)

$$q_{CHW}(t) = q_{CRAH}(t) + q_{g,CRAH,\,fan}(t) \tag{A8}$$

$$f_{CHW,pump}(t) = \frac{q_{CHW}(t)}{\rho_w c_{p,w} \Delta T_{CHW}} \tag{A9}$$

$$PR_{CHW}(t) = \frac{f_{CHW,pump}(t)}{f_{d,CHW,\,pump}} \tag{A10}$$

$$P_{CHW,\,pump}(t) = P_{d,CHW,pump} \times \left(a + b{\cdot}PR_{CHW}(t) + c{\cdot}PR_{CHW}(t)^2 + d{\cdot}PR_{CHW}(t)^3\right) \tag{A11}$$

Appendix A.2.3. Chiller

$$q_{chiller}(t) = q_{CHW}(t) \tag{A12}$$

$$PLR(t) = \frac{q_{chiller}(t)}{q_{chiller,avail}(t)} \tag{A13}$$

$$q_{chiller,avail}(t) = CAPFT(t) \times q_{d,chiller} \tag{A14}$$

$$CAPFT(t) = a + b{\cdot}T_{CHW,C} + c{\cdot}T_{CHW,C}^2 + d{\cdot}T_{CW,C}(t) + e{\cdot}T_{CW,C}(t)^2 + f{\cdot}T_{CHW,C}{\cdot}T_{CW,C}(t) \tag{A15}$$

$$EIRFPLR(t) = a + b{\cdot}PLR(t) + c{\cdot}PLR(t)^2 \tag{A16}$$

$$EIRFT(t) = a + b{\cdot}T_{CHW,C} + c{\cdot}T_{CHW,C}^2 + d{\cdot}T_{CW,C}(t) + e{\cdot}T_{CW,C}(t)^2 + f{\cdot}T_{CHW,C}{\cdot}T_{CW,C}(t) \tag{A17}$$

$$P_{comp}(t) = P_{d,comp} \times CAPFT(t) \times EIRFPLR(t) \times EIRFT(t) \tag{A18}$$

Appendix A.2.4. Cooling Water Loop (Cooling Water Pump)

$$q_{CW}(t) = q_{chiller}(t) + q_{g,comp}(t) \tag{A19}$$

$$f_{CW,pump}(t) = \frac{q_{CW}(t)}{\rho_w c_{p,w} \Delta T_{CW}} \tag{A20}$$

$$PR_{CW}(t) = \frac{f_{CW,pump}(t)}{f_{d,CW,\ pump}} \tag{A21}$$

$$P_{CW,\ pump}(t) = P_{d,CW,pump} \times \left(a + b{\cdot}PR_{CW}(t) + c{\cdot}PR_{CW}(t)^2 + d{\cdot}PR_{CW}(t)^3\right) \tag{A22}$$

Appendix A.2.5. Cooling Tower

$$\begin{aligned}
T_{approach}(t) &= Y\left(T_{OWB}(t), T_{range}(t), PR_{CW}(t), FPR_{CT}(t)\right) \\
&= \beta_1 + \beta_2 T_{OWB}(t) + \beta_3 T_{OWB}(t)^2 + \beta_4 T_{range}(t + \beta_5 T_{OWB}(t) T_{range}(t) \\
&+\beta_6 T_{OWB}(t)^2 T_{range}(t) + \beta_7 T_{range}(t)^2 + \beta_8 T_{OWB}(t) T_{range}(t)^2 + \beta_9 T_{OWB}(t)^2 T_{range}(t)^2 \\
&+\beta_{10} \frac{PR_{CW}(t)}{FPR_{CT}(t)} + \beta_{11} T_{OWB}(t) \frac{PR_{CW}(t)}{FPR_{CT}(t)} + \beta_{12} T_{OWB}(t)^2 \frac{PR_{CW}(t)}{FPR_{CT}(t)} \\
&+\beta_{13} T_{range}(t) \frac{PR_{CW}(t)}{FPR_{CT}(t)} + \beta_{14} T_{OWB}(t) T_{range}(t) \frac{PR_{CW}(t)}{FPR_{CT}(t)} \\
&+\beta_{15} T_{OWB}(t)^2 T_{range}(t) \frac{PR_{CW}(t)}{FPR_{CT}(t)} + \beta_{16} T_{range}(t)^2 \frac{PR_{CW}(t)}{FPR_{CT}(t)} \\
&+\beta_{17} T_{OWB}(t) T_{range}(t)^2 \frac{PR_{CW}(t)}{FPR_{CT}(t)} + \beta_{18} T_{OWB}(t)^2 T_{range}(t)^2 \frac{PR_{CW}(t)}{FPR_{CT}(t)} + \beta_{19} \frac{PR_{CW}(t)}{FPR_{CT}(t)}^2 \\
&+\beta_{20} T_{OWB}(t) \frac{PR_{CW}(t)}{FPR_{CT}(t)}^2 + \beta_{21} T_{OWB}(t)^2 \frac{PR_{CW}(t)}{FPR_{CT}(t)}^2 + \beta_{22} T_{range}(t) \frac{PR_{CW}(t)}{FPR_{CT}(t)}^2 \\
&+\beta_{23} T_{OWB}(t) T_{range}(t) \frac{PR_{CW}(t)}{FPR_{CT}(t)}^2 + \beta_{24} T_{OWB}(t)^2 T_{range}(t) \frac{PR_{CW}(t)}{FPR_{CT}(t)}^2 \\
&+\beta_{25} T_{range}(t)^2 \frac{PR_{CW}(t)}{FPR_{CT}(t)}^2 + \beta_{26} T_{OWB}(t) T_{range}(t)^2 \frac{PR_{CW}(t)}{FPR_{CT}(t)}^2 \\
&+\beta_{27} T_{OWB}(t)^2 T_{range}(t)^2 \frac{PR_{CW}(t)}{FPR_{CT}(t)}^2
\end{aligned} \tag{A23}$$

$$P_{CT,fan}(t) = \left\{P_{d,CTfan} \times \left(a + b{\cdot}FPR_{CT}(t) + c{\cdot}FPR_{CT}(t)^2 + d{\cdot}FPR_{CT}(t)^3\right\} \times FanPLR(t)\right. \tag{A24}$$

To calculate $FPR_{CT}(t)$ and $FanPLR(t)$ for the cooling tower fan, the following four steps are performed.

Step 1:

① Calculate the cooling water supply temperature when the cooling tower fan is operated at maximum speed ($T_{CW,C,fanMAX}(t)$).

② Compare it with the cooling water supply set temperature ($T_{d,CW,C}$). If the calculated temperature is higher, the cooling tower fan operates at maximum speed. If it is lower, proceed to Step 2.

$$T_{CW,C,fanMAX}(t) = T_{OWB}(t) + T_{approach}(t) = T_{CW,H}(t) + T_{range}(t) \tag{A25}$$

$$T_{CW,C}(t) = T_{CW,C,fanMAX}(t) \tag{A26}$$

$$FPR_{CT}(t) = \frac{f_{CT,fan}(t)}{f_{d,CT}} = 1 \tag{A27}$$

$$FanPLR(t) = 1 \tag{A28}$$

Note that the approach temperature correlation as described previously is a function of range temperature, so the equations above must be solved iteratively to converge on a solution.

Step 2:

① Calculate the cooling water supply temperature when the cooling tower fan is in the off state, called "free convection" ($T_{CW,C,fanOFF}$(t)).

② Compare it with the cooling water supply set temperature ($T_{d,CW,C}$). If the calculated temperature is lower, the cooling tower fan is off. If it is higher, proceed to Step 3.

$$T_{CW,C,fanOFF}(t) = T_{CW,H}(t) - \left\{ Frac_{freeconv}\left(T_{CW,H}(t) - T_{CW,C,fanMAX}(t) \right) \right\} \quad \text{(A29)}$$

$$T_{CW,C}(t) = T_{CW,C,fanOFF}(t) \quad \text{(A30)}$$

$$FPR_{CT}(t) = \frac{f_{CT,fan}(t)}{f_{d,CT}} = 0 \quad \text{(A31)}$$

$$FanPLR(t) = 0 \quad \text{(A32)}$$

where, $Frac_{freeconv}$ is the fraction of tower capacity in Free Convection Regime, Default value is 0.125

Step 3:

① Calculate the cooling water supply temperature when the cooling tower fan is operated at minimum speed ($T_{CW,C,fanMIN}(t)$).

② Compare it with the cooling water supply set temperature ($T_{d,CW,C}$). If the calculated temperature is lower, the cooling tower fan operates in an on-and-off mode to control the cooling water supply temperature to the desired setpoint. If it is higher, proceed to Step 4.

$$T_{CW,C,fanMIN}(t) = T_{OWB}(t) + T_{approach}(t) = T_{CW,H}(t) + T_{range}(t) \quad \text{(A33)}$$

$$T_{CW,C}(t) = T_{d,CW,C} = T_{OWB}(t) + T_{approach}(t) \quad \text{(A34)}$$

$$FPR_{CT}(t) = \frac{f_{CT,fanMin}(t)}{f_{d,CT}} \ (Default: 0.2) \quad \text{(A35)}$$

$$FanPLR(t) = \frac{T_{CW,C,fanOFF}(t) - T_{d,CW,C}}{T_{CW,C,fanOFF}(t) - T_{CW,C,fanMIN}(t)} \quad \text{(A36)}$$

Note that the approach temperature correlation as described previously is a function of range temperature, so the equations above must be solved iteratively to converge on a solution.

Step 4:

① The cooling tower fan is controlled to maintain the cooling water supply temperature at the desired setpoint ($T_{d,CW,C}$).

② Calculate the speed of the cooling tower fan to achieve the desired cooling water supply temperature.

$$T_{CW,C}(t) = T_{d,CW,C} \quad \text{(A37)}$$

$$T_{approach}(t) = T_{d,CW,C} - T_{OWB}(t) = Y\left(T_{OWB}(t), T_{range}(t), PR_{CW}(t), FPR_{CT}(t)\right) \quad \text{(A38)}$$

$$FanPLR(t) = 1 \quad \text{(A39)}$$

Appendix A.3. DASE Model

Appendix A.3.1. Free Cooling Mode

$$q_{CRAH}(t) = q_{cooling}(t) \quad \text{(A40)}$$

The process for calculating the power of the CRAH fan is the same as described in section Appendix A.2.2.

The heat ($q_{CRAH}(t)$) that needs to be removed from the CRAH fan and the heat ($q_{g,CRAH,\ fan}(t)$) generated by the CRAH fan should be eliminated through the introduction of outdoor air facilitated by the exhaust fan.

$$q_{DASE}(t) = q_{CRAH}(t) + q_{g,CRAH,\ fan}(t) \tag{A41}$$

$$f_{EA,\ fan}(t) = \frac{q_{DASE}(t)}{\rho_a c_{p,a}(T_{CRAH,H} - T_{ODB}(t))} \tag{A42}$$

$$FR_{EA}(t) = \frac{f_{EA,\ fan}(t)}{f_{d,\ EA\ fan}} \tag{A43}$$

$$FP_{EA,fan}(t) = P_{d,EA\ fan} \times \left(a + b{\cdot}FR_{EA}(t) + c{\cdot}FR_{EA}(t)^2 + d{\cdot}FR_{EA}(t)^3\right) \tag{A44}$$

Appendix A.3.2. Mixed Cooling Mode

$$q_{CRAH}(t) = q_{cooling}(t) \tag{A45}$$

The process for calculating the power of the CRAH fan is the same as described in section Appendix A.2.2.

The remaining heat ($q_{CRAH}(t) + q_{g,CRAH,\ fan}(t) - q_{DASE}(t)$) after accounting for the heat ($q_{DASE}(t)$) removed by operating the exhaust fan at maximum airflow should be eliminated from the Chilled Water loop, chiller, and Cooling Water loop.

$$q_{DASE}(t) = \rho_a{\cdot}c_{p,a}{\cdot}f_{d,\ EAfan}(T_{CRAH,H} - T_{ODB}(t)) \tag{A46}$$

$$q_{CHW}(t) = q_{CRAH}(t) + q_{g,CRAH,\ fan}(t) - q_{DASE}(t) \tag{A47}$$

$$q_{chiller}(t) = q_{CHW}(t) \tag{A48}$$

$$q_{CW}(t) = q_{chiller}(t) + q_{g,comp}(t) \tag{A49}$$

The process for calculating the power of the CHW pump, chiller, CW pump, and cooling tower is the same as described in sections from Appendices A.2.3–A.2.5.

Appendix A.4. IASE Model

Appendix A.4.1. Free Cooling Mode

$$q_{CRAH}(t) = q_{cooling}(t) \tag{A50}$$

The process for calculating the power of the CRAH fan is the same as described in section Appendix A.2.2.

The heat that needs to be removed from the CRAH fan ($q_{CRAH}(t)$) and the heat generated by the fan itself ($q_{g,CRAH,\ fan}(t)$) should be eliminated by utilizing an air-to-air heat exchanger that facilitates heat exchange with the outside air.

$$q_{IASE}(t) = q_{CRAH}(t) + q_{g,CRAH,\ fan}(t) \tag{A51}$$

$$f_{EA,\ fan}(t) = \frac{q_{IASE}(t)}{\epsilon_{AHX}\rho_a c_{p,a}(T_{CRAH,H} - T_{ODB}(t))} \tag{A52}$$

$$FR_{EA}(t) = \frac{f_{EA,\ fan}(t)}{f_{d,\ EA\ fan}} \tag{A53}$$

$$FP_{EA,fan}(t) = P_{d,EA\ fan} \times \left(a + b{\cdot}FR_{EA}(t) + c{\cdot}FR_{EA}(t)^2 + d{\cdot}FR_{EA}(t)^3\right) \tag{A54}$$

Appendix A.4.2. Mixed Cooling Mode

$$q_{CRAH}(t) = q_{cooling}(t) \tag{A55}$$

The process for calculating the power of the CRAH fan is the same as described in section Appendix A.2.2.

The remaining heat ($q_{CRAH}(t) + q_{g,CRAH,\,fan}(t) - q_{IASE}(t)$) after accounting for the heat ($q_{IASE}(t)$) removed by operating the exhaust fan at maximum airflow should be taken care of by removing it from the Chilled Water loop, chiller, and Cooling Water loop.

$$q_{IASE}(t) = \epsilon_{AHX} \cdot \rho_a \cdot c_{p,a} \cdot f_{d,\,EAfan}(T_{CRAH,H} - T_{ODB}(t)) \tag{A56}$$

$$q_{CHW}(t) = q_{CRAH}(t) + q_{g,CRAH,\,fan}(t) - q_{IASE}(t) \tag{A57}$$

$$q_{chiller}(t) = q_{CHW}(t) \tag{A58}$$

$$q_{CW}(t) = q_{chiller}(t) + q_{g,comp}(t) \tag{A59}$$

The process for calculating the power of the CHW pump, chiller, CW pump, and cooling tower is the same as described in sections from Appendices A.2.3–A.2.5.

Appendix A.5. WSE Model

Appendix A.5.1. Free Cooling Mode

The heat that needs to be removed from the chilled water loop should be eliminated by utilizing a cooling tower.

$$q_{CRAH}(t) = q_{cooling}(t) \tag{A60}$$

$$q_{CHW}(t) = q_{CRAH}(t) + q_{g,CRAH,\,fan}(t) \tag{A61}$$

$$q_{WSE}(t) = q_{CHW}(t) \tag{A62}$$

$$q_{CW}(t) = q_{WSE}(t) \tag{A63}$$

The process for calculating the power of the CRAH fan, CHW pump, CW pump, and cooling tower is the same as described in sections Appendix A.2.2, Appendix A.2.3, and Appendix A.2.5.

When calculating Appendix A.2.5, replace $T_{d,CW,C}$ with $T_{CW,C,WSE}(t)$ for the calculations Appendix A.2.5.

$$\begin{array}{c} T_{CW,C,WSE}(t) = T_{CHW,H}(t) - \frac{f_{CHW,pump}(t)(T_{CHW,H}(t) - T_{CHW,C}(t))}{\epsilon_{WHX} \cdot f_{CW,pump}(t)} \\ when, \quad f_{CW,pump}(t) \le f_{CHW,pump}(t) \\ T_{d,CW,C} = T_{CW,C}(t) = T_{CHW,H}(t) - \frac{T_{CHW,H}(t) - T_{CHW,C}(t)}{\epsilon_{WHX}} \\ when, \quad f_{CW,pump}(t) \ge f_{CHW,pump}(t) \end{array} \tag{A64}$$

Appendix A.5.2. Mixed Cooling Mode

$$q_{CRAH}(t) = q_{cooling}(t) \tag{A65}$$

$$q_{CHW}(t) = q_{CRAH}(t) + q_{g,CRAH,\,fan}(t) \tag{A66}$$

The process for calculating the power of the CRAH fan and CHW pump is the same as described in section Appendices A.2.2 and A.2.3.

The remaining heat ($q_{CHW}(t) - q_{WSE}(t)$) after considering the heat extracted by operating the cooling water pump and cooling tower fan at maximum airflow should be removed from the chiller.

$$q_{WSE}(t) = \epsilon_{WHX} \cdot \rho_w \cdot c_{p,w} \cdot f_{d,CW,\,pump}(T_{CHW,H} - T_{CW,C}(t)) \tag{A67}$$

$$q_{chiller}(t) = q_{CHW}(t) - q_{WSE}(t) \quad \text{(A68)}$$

$T_{CW,C}(t)$ is calculated by assuming $PR_{CW}(t) = 1$, $FPR_{CT}(t) = 1$, and then applying YorkCalc calculation method.

In Mixed Cooling mode, the cooling water supply temperature (($T_{CW,C}(t)$) is determined by assuming $PR_{CW}(t) = 1$, $PR_{CW}(t) = 1$, and then applying YorkCalc calculation method.

$$T_{CW,C}(t) = T_{OWB}(t) + T_{approach}(t) \quad \text{(A69)}$$

$$T_{approach}(t) = Y\left(T_{OWB}(t), T_{range}(t), PR_{CW}(t), FPR_{CT}(t)\right) \quad \text{(A70)}$$

Appendix B

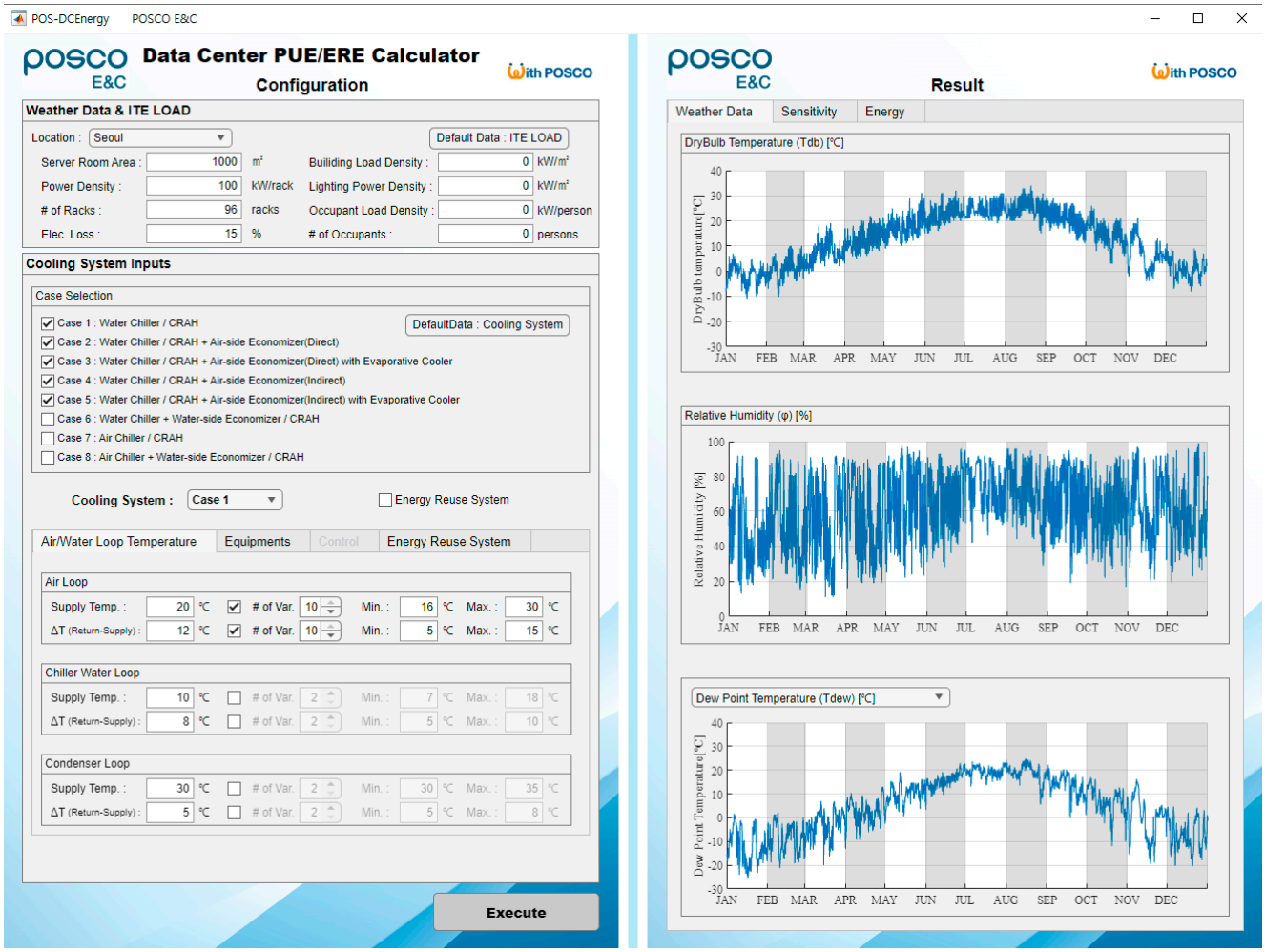

(a)

Figure A1. *Cont.*

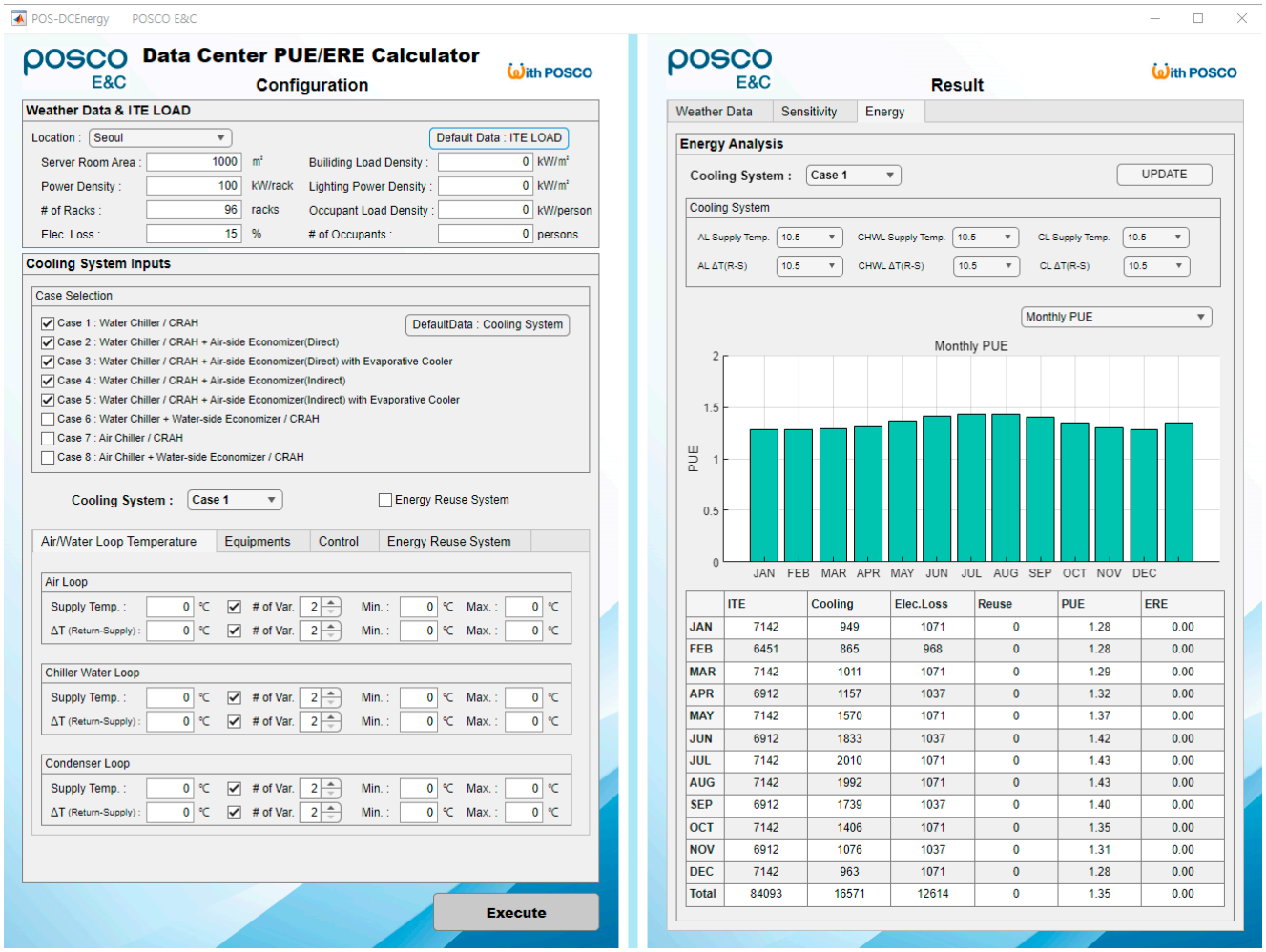

(**b**)

Figure A1. Input and output windows of the DCSim (**a**) Input window and weather data output window; (**b**) Input window and PUE results output window.

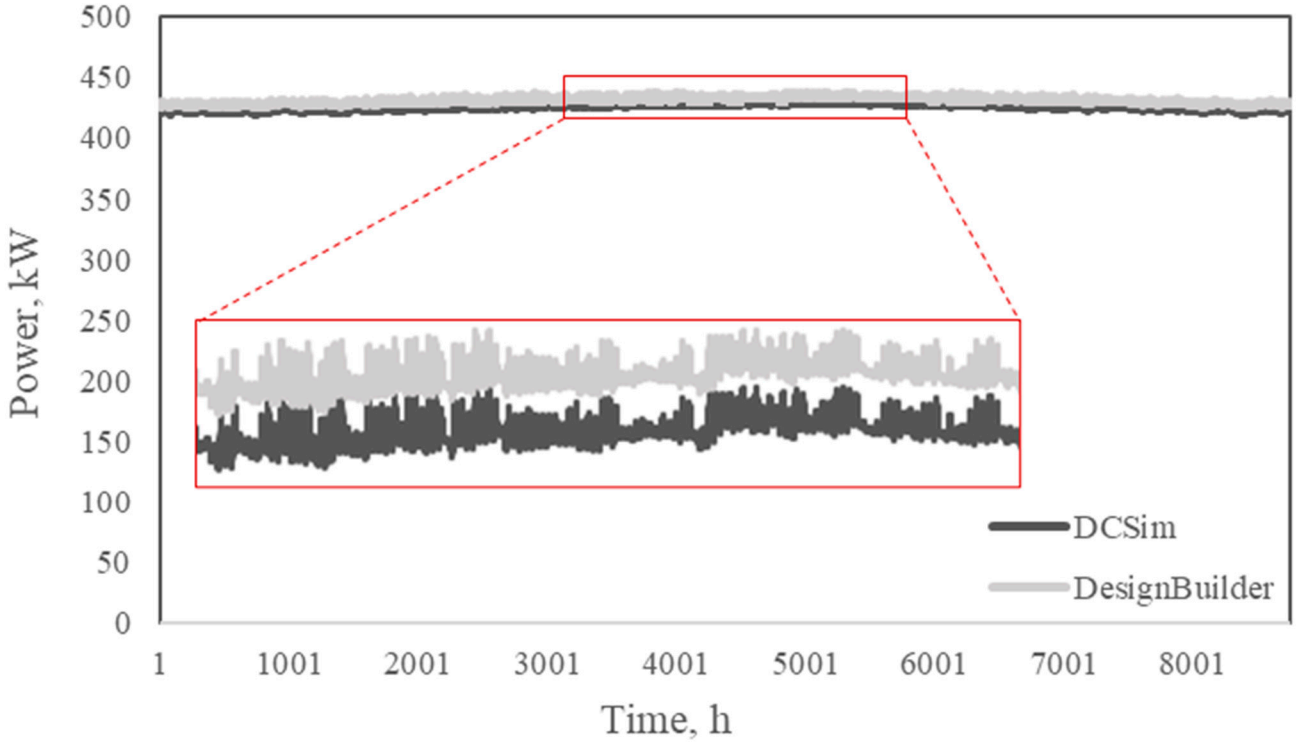

(**a**)

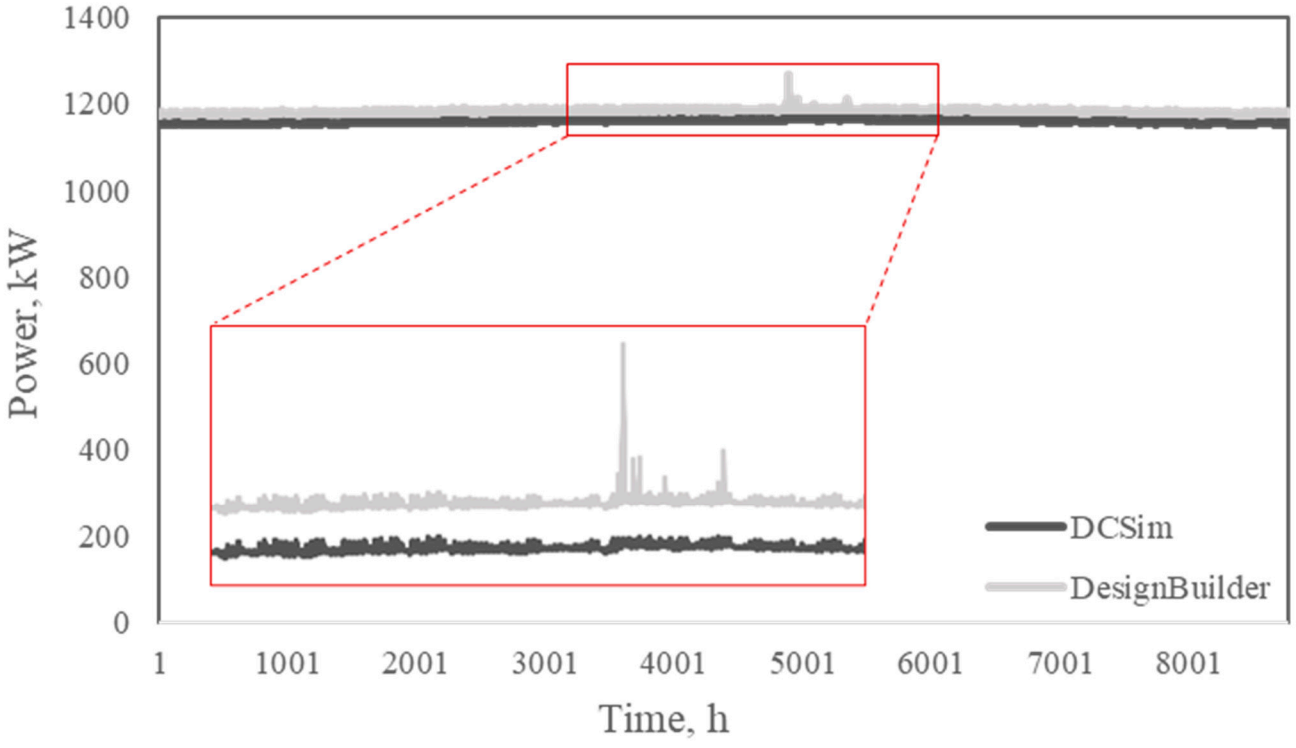

(**b**)

Figure A2. *Cont.*

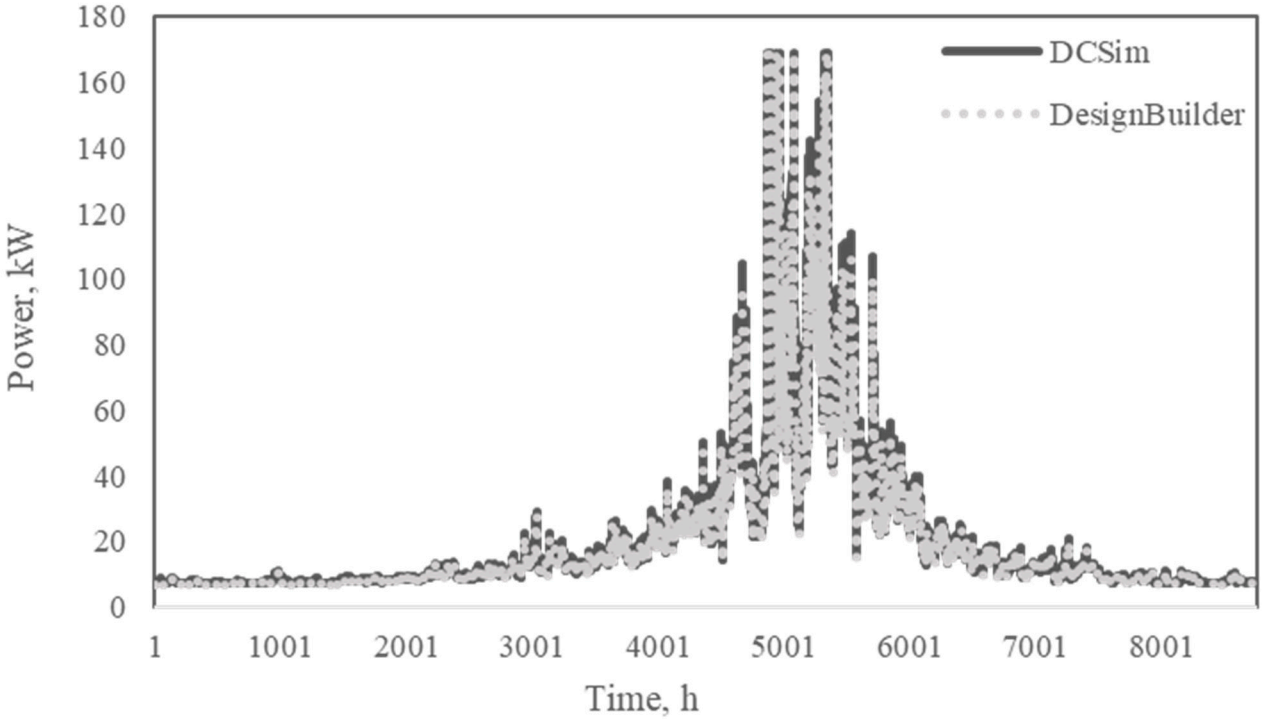

(**c**)

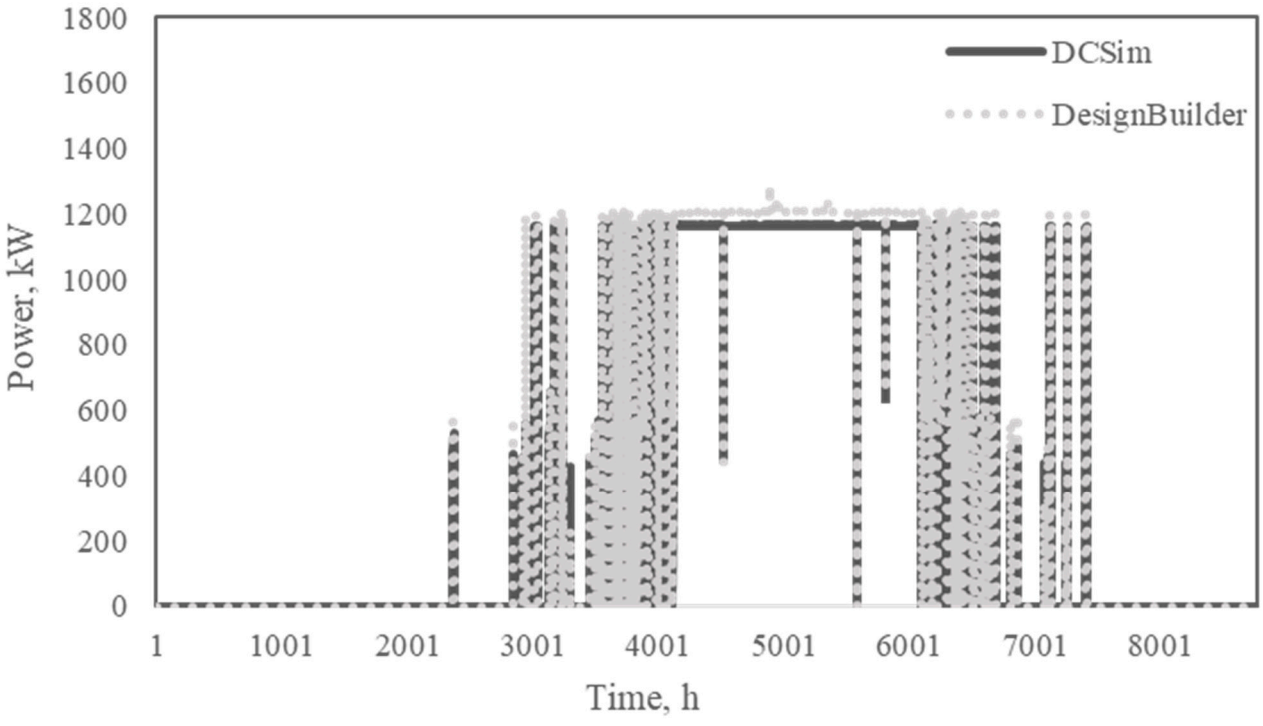

(**d**)

Figure A2. *Cont.*

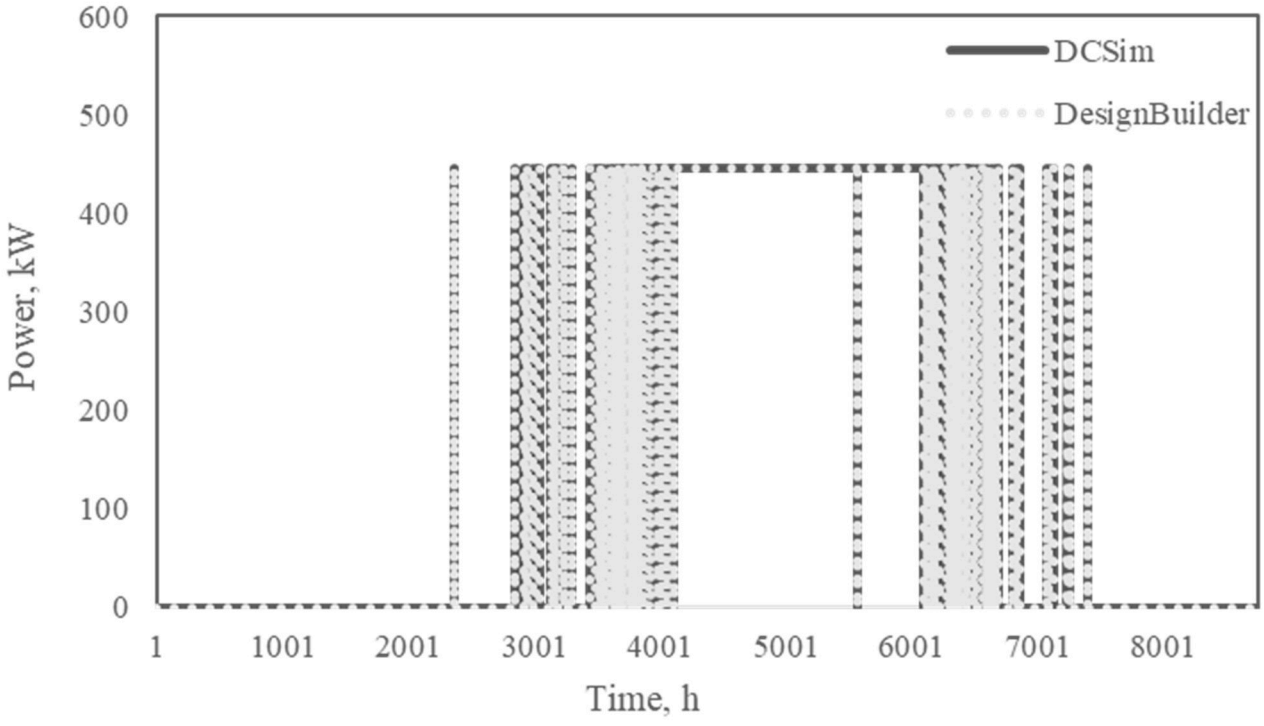

(**e**)

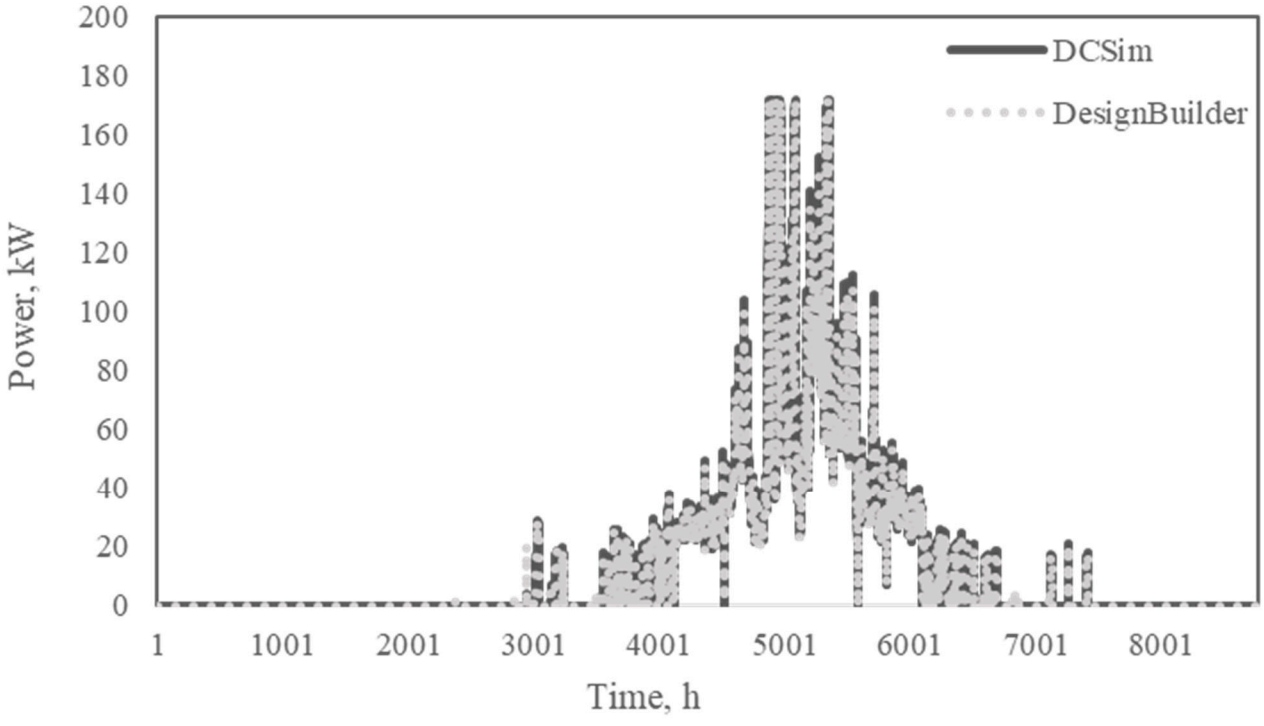

(**f**)

Figure A2. Hourly power consumption of equipment: (**a**) CRAH fan (Baseline); (**b**) Chiller (Baseline); (**c**) Cooling tower fan (Baseline); (**d**) Chiller (DASE); (**e**) Pumps (DASE); (**f**) Cooling tower fan (DASE).

References

1. IEA. *Data Centres and Data Transmission Networks*; IEA: Paris, France, 2022. Available online: https://www.iea.org/reports/data-centres-and-data-transmission-networks (accessed on 9 January 2024).
2. Masanet, E.; Shehabi, A.; Lei, N.; Smith, S.; Koomey, J. Recalibrating global data center energy-use estimates. *Science* **2020**, *367*, 984–986. [CrossRef] [PubMed]
3. Ebrahimi, K.; Jones, G.F.; Fleischer, A.S. A review of data center cooling technology, operating conditions and the corresponding low-grade waste heat recovery opportunities. *Renew. Sustain. Energy Rev.* **2014**, *31*, 622–638. [CrossRef]
4. Malmodin, J.; Lövehagen, N.; Bergmark, P.; Lundén, D. ICT sector electricity consumption and greenhouse gas emissions-2020 tutcome. *Telecommun. Policy* **2023**, 102701.
5. Zhu, H.; Zhang, D.; Goh, H.H.; Wang, S.; Ahmad, T.; Mao, D.; Liu, T.; Zhao, H.; Wu, T. Future data center energy-conservation and emission-reduction technologies in the context of smart and low-carbon city construction. *Sustain. Cities Soc.* **2023**, *89*, 104322. [CrossRef]
6. Isazadeh, A.; Ziviani, D.; Claridge, D.E. Global trends, performance metrics, and energy reduction measures in datacom facilities. *Renew. Sustain. Energy Rev.* **2023**, *174*, 113149. [CrossRef]
7. Belady, C.; Rawson, A.; Pfleuger, D.; Cader, T. *Green Grid Data Center Power Efficiency Metrics: PUE and DCiE*; Whitepaper # 6; The Green Grid: Washington, DC, USA, 2008.
8. Mahdavi, R. *Seventh Floor Data Centers RAY Building, Saint Louis, Missouri, Energy Usage Efficiency Assessment Report*; Lawrence Berkeley National Laboratory: Berkeley, CA, USA, 2014; p. 39.
9. Shehabi, A.; Smith, S.; Sartor, D.; Brown, R.; Herrlin, M.; Koomey, J.; Masanet, E.; Horner, N.; Azevedo, I.; Lintner, W. *United States Data Center Energy Usage Report*; LBNL–1005775; Lawrence Berkeley National Laboratory: Berkeley, CA, USA, 2016.
10. Dayarathna, M.; Wen, Y.; Fan, R. Data center energy consumption modeling: A survey. *IEEE Commun. Surv. Tutor.* **2015**, *18*, 732–794. [CrossRef]
11. Tibaldi, M.; Pilato, C. A Survey of FPGA Optimization Methods for Data Center Energy Efficiency. *IEEE Trans. Sustain. Comput.* **2023**, *8*, 343–362. [CrossRef]
12. Cho, J.; Jeong, C.; Kim, B.S. Study on load-profiles and energy consumption for the optimal IT environment control in the (internet) data center. *J. Archit. Inst. Korea* **2007**, *23*, 209–216.
13. Ham, S.W.; Park, J.S.; Jeong, J.W. Optimum supply air temperature ranges of various air-side economizers in a modular data center. *Appl. Therm. Eng.* **2015**, *77*, 163–179. [CrossRef]
14. Oró, E.; Depoorter, V.; Pflugradt, N.; Salom, J. Overview of direct air free cooling and thermal energy storage potential energy savings in data centres. *Appl. Therm. Eng.* **2015**, *85*, 100–110. [CrossRef]
15. Lee, K.P.; Chen, H.L. Analysis of energy saving potential of air-side free cooling for data centers in worldwide climate zones. *Energy Build.* **2013**, *64*, 103–112. [CrossRef]
16. Kim, J.Y.; Chang, H.J.; Jung, Y.H.; Cho, K.M.; Augenbroe, G. Energy conservation effects of a multi-stage outdoor air enabled cooling system in a data center. *Energy Build.* **2017**, *138*, 257–270. [CrossRef]
17. Ham, S.W.; Kim, M.H.; Choi, B.N.; Jeong, J.W. Energy saving potential of various air-side economizers in a modular data center. *Appl. Energy* **2015**, *138*, 258–275. [CrossRef]
18. Deymi-Dashtebayaz, M.; Namanlo, S.V. Potentiometric and economic analysis of using air and water-side economizers for data center cooling based on various weather conditions. *Int. J. Refrig.* **2019**, *99*, 213–225. [CrossRef]
19. Deymi-Dashtebayaz, M.; Valipour Namanlo, S.; Arabkoohsar, A. Simultaneous use of air-side and water-side economizers with the air source heat pump in a data center for cooling and heating production. *Appl. Therm. Eng.* **2019**, *161*, 114133. [CrossRef]
20. Díaz, A.J.; Cáceres, R.; Torres, R.; Cardemil, J.M.; Silva-Llanca, L. Effect of climate conditions on the thermodynamic performance of a data center cooling system under water-side economization. *Energy Build.* **2020**, *208*, 109634. [CrossRef]
21. Agrawal, A.; Khichar, M.; Jain, S. Transient simulation of wet cooling strategies for a data center in worldwide climate zones. *Energy Build.* **2016**, *127*, 352–359. [CrossRef]
22. Li, J.; Li, Z. Model-based optimization of free cooling switchover temperature and cooling tower approach temperature for data center cooling system with water-side economizer. *Energy Build.* **2020**, *227*, 110407. [CrossRef]
23. Zhang, Y.; Wei, Z.; Zhang, M. Free cooling technologies for data centers: Energy saving mechanism and applications. *Energy Procedia* **2017**, *143*, 410–415. [CrossRef]
24. Cheung, H.; Wang, S. Optimal design of data center cooling systems concerning multi-chiller system configuration and component selection for energy-efficient operation and maximized free-cooling. *Renew. Energy* **2019**, *143*, 1717–1731. [CrossRef]
25. Habibi Khalaj, A.; Abdulla, K.; Halgamuge, S.K. Towards the stand-alone operation of data centers with free cooling and optimally sized hybrid renewable power generation and energy storage. *Renew. Sustain. Energy Rev.* **2018**, *93*, 451–472. [CrossRef]
26. Zhang, H.; Shao, S.; Xu, H.; Zou, H.; Tian, C. Free cooling of data centers: A review. *Renew. Sustain. Energy Rev.* **2014**, *35*, 171–182. [CrossRef]
27. Xu, S.; Zhang, H.; Wang, Z. Thermal Management and Energy Consumption in Air, Liquid, and Free Cooling Systems for Data Centers: A Review. *Energies* **2023**, *16*, 1279. [CrossRef]
28. ASHRAE Technical Committee 9.9. *Thermal Guidelines for Data Processing Environments*, 4th ed.; ASHRAE: Atlanta, GA, USA, 2015.

29. Gözcü, O.; Özada, B.; Carfi, M.U.; Erden, H.S. Worldwide energy analysis of major free cooling methods for data centers. In Proceedings of the 2017 16th IEEE Intersociety Conference on Thermal and Thermomechanical Phenomena in Electronic Systems (ITherm), Orlando, FL, USA, 30 May–2 June 2017; pp. 968–976.
30. Kim, M.H.; Ham, S.W.; Park, J.S.; Jeong, J.W. Impact of integrated hot water cooling and desiccant-assisted evaporative cooling systems on energy savings in a data center. *Energy* **2014**, *78*, 384–396. [CrossRef]
31. Brady, G.A.; Kapur, N.; Summers, J.L.; Thompson, H.M. A case study and critical assessment in calculating power usage effectiveness for a data centre. *Energy Convers. Manag.* **2013**, *76*, 155–161. [CrossRef]
32. Chen, H.; Cheng, W.L.; Zhang, W.W.; Peng, Y.H.; Jiang, L.J. Energy saving evaluation of a novel energy system based on spray cooling for supercomputer center. *Energy* **2017**, *141*, 304–315. [CrossRef]
33. Cho, J.; Kim, Y. Improving energy efficiency of dedicated cooling system and its contribution towards meeting an energy-optimized data center. *Appl. Energy* **2016**, *165*, 967–982. [CrossRef]
34. Cho, J.; Yang, J.; Lee, C.; Lee, J. Development of an energy evaluation and design tool for dedicated cooling systems of data centers: Sensing data center cooling energy efficiency. *Energy Build.* **2015**, *96*, 357–372. [CrossRef]
35. Lei, N.; Masanet, E. Statistical analysis for predicting location-specific data center PUE and its improvement potential. *Energy* **2020**, *201*, 117556. [CrossRef]
36. Song, Z.; Zhang, X.; Eriksson, C. Data Center Energy and Cost Saving Evaluation. *Energy Procedia* **2015**, *75*, 1255–1260. [CrossRef]
37. Chen, L.; Wemhoff, A.P. The sustainability benefits of economization in data centers containing chilled water systems. *Resour. Conserv. Recycl.* **2023**, *196*, 107053. [CrossRef]
38. ASHRAE. *ANSI/ASHRAE 169-2020: Climatic Data for Building Design Standards*; ASHRAE: Peachtree Corners, GA, USA, 2021.
39. Mi, R.; Bai, X.; Xu, X.; Ren, F. Energy performance evaluation in a data center with water-side free cooling. *Energy Build.* **2023**, *295*, 113278. [CrossRef]
40. ASHRAE. *Datacom Equipment Power Trends and Cooling Applications*; American Society of Heating, Refrigerating and Air-conditioning Engineers, Inc.: Atlanta, GA, USA, 2012; p. 7.
41. DOE. *EnergyPlus Version 9.2.0 Documentation: Engineering Reference*; U.S. DOE: Washington, DC, USA, 2019; Chapter 16.
42. ASHRAE. *Guideline 14-2014: Measurement of Energy, Demand, and Savings*; ASHRAE: Atlanta, GA, USA, 2014.
43. DOE. EnergyPlus. Available online: https://energyplus.net/weather (accessed on 15 July 2023).
44. Joshi, Y.; Kumar, P. *Energy Efficient Thermal Management of Data Centers*; Springer: New York, NY, USA, 2012.
45. ASHRAE. *Liquid Cooling Guidelines for Datacom Equipment Centers*; ASHRAE: Atlanta, GA, USA, 2014.
46. National Renewable Energy Laboratory (NREL). Data Center Efficiency Dashboard. Available online: https://www.nrel.gov/hpc/cool.html (accessed on 4 June 2023).